Impact of Spike Train Autostructure on Probability Distribution of Joint Spike Events

Gordon Pipa
gpipa@uos.de
Institute of Cognitive Science, University of Osnabrück, 49069 Osnabrück,
Germany

Sonja Grün
s.gruen@fz-juelich.de
Institute of Neuroscience and Medicine (INM-6), Computational and Systems
Neuroscience, Forschungszentrum Jülich, 52428 Jülich, Germany; Institute
for Advanced Simulation (IAS-6), Theoretical Neuroscience, Forschungszentrum
Jülich, 52428 Jülich, Germany; Theoretical Systems Neurobiology, RWTH Aachen
University, 52056 Aachen, Germany; and RIKEN Brain Science Institute,
2-1 Hirosawa, Wako-shi, Saitama 351-0198, Japan

Carl van Vreeswijk
cornelis.van-vreeswijk@univ-paris5.fr
Université Paris Descartes, Laboratoire de Neurophysique et Physiologie, CNRS,
75270 Paris Cedex 06, France

The discussion whether temporally coordinated spiking activity really exists and whether it is relevant has been heated over the past few years. To investigate this issue, several approaches have been taken to determine whether synchronized events occur significantly above chance, that is, whether they occur more often than expected if the neurons fire independently. Most investigations ignore or destroy the autostructure of the spiking activity of individual cells or assume Poissonian spiking as a model. Such methods that ignore the autostructure can significantly bias the coincidence statistics. Here, we study the influence of the autostructure on the probability distribution of coincident spiking events between tuples of mutually independent non-Poisson renewal processes. In particular, we consider two types of renewal processes that were suggested as appropriate models of experimental spike trains: a gamma and a log-normal process. For a gamma process, we characterize the shape of the distribution analytically with the Fano factor (FF_c). In addition, we perform Monte Carlo estimations to derive the full shape of the distribution and the probability for false positives if a different process type is assumed as was actually present. We also determine how manipulations of such spike trains, here dithering, used for the generation of surrogate

data change the distribution of coincident events and influence the significance estimation. We find, first, that the width of the coincidence count distribution and its FF_c depend critically and in a nontrivial way on the detailed properties of the structure of the spike trains as characterized by the coefficient of variation C_V. Second, the dependence of the FF_c on the C_V is complex and mostly nonmonotonic. Third, spike dithering, even if as small as a fraction of the interspike interval, can falsify the inference on coordinated firing.

1 Introduction

Synchronous spiking has been implicated in neural coding (Abeles, Bergman, Margalit, & Vaadia, 1993; Gray, König, Engel, & Singer, 1989; Kilavik et al., 2009; Riehle, Grün, Diesmann, & Aertsen, 1997; Singer, 1999). It has been associated with cortical avalanches (Beggs & Plenz, 2003) and synfire chains (Abeles, 1991) and has also been used to constrain the mechanisms that give rise to cortical activity (Diesmann, Gewaltig, & Aertsen, 1999; Gutkin, Laing, Colby, Chow, & Ermentrout, 2001; Vicente, Gollo, Mirasso, Fischer, & Pipa, 2008; Sommer & Wennekers, 2001; Aoki & Aoyagi, 2007). Hence the determination of whether synchronized events occur above chance (i.e. whether they occur more often than expected if the neurons fire independently) has recently attracted considerable attention. Several approaches have been taken to investigate this issue (Amari, Nakahara, Wu, & Sakai, 2003; Aertsen, Gerstein, Habib, & Palm, 1989; Brody, 1999; Brown, Kass, & Mitra, 2004; Truccolo, Eden, Fellows, Donoghue, & Brown, 2005; Gerstein & Perkel, 1972; Grün, Diesmann, Grammont, Riehle, & Aertsen, 1999; Grün, Diesmann, & Aertsen, 2002a, 2002c; Grün, 2009; Ikegaya et al., 2004; Kass, Ventura, & Brown, 2005; König, 1994; Louis, Gerstein, Grün, & Diesmann, 2010; Pipa & Grün, 2003; Pipa, Riehle, & Grün, 2007; Pipa, Wheeler, Singer, & Nikolic, 2008; Agmon, 2012; Ventura, Cai, & Kass, 2005; Gerhard, Haslinger, & Pipa, 2011a, 2011b; Pipa & Munk, 2011; Wu, Wheeler, & Pipa, 2011) (Oram, Wiener, Lestienne, & Richmond, 1999) performed a similar analysis, however, for patterns within single spike trains). Many of these approaches for the analysis of correlated spike trains imply more or less implicitly the assumption of Poisson spike trains, for example, by simulating spike trains as Poisson processes with the same rate profiles as the neurons under investigation to determine the statistics of coincident events analytically. However, experimental interspike interval (ISI) distributions can show a substantial deviation from the exponential distribution, since the nature of experimental spike trains can be dramatically different from Poisson processes (Burns & Webb, 1976; Levine, 1991; Teich, Heneghan, Lowen, Ozaki, & Kaplan, 1997; Iyengar & Liao, 1997; Nawrot et al., 2007, 2008; Smith, 1954a, 1954b; Krahe & Gabbiani, 2004; Farkhooi, Strube-Bloss, & Nawrot, 2009). However, their effect on the occurrence of synchronous or spatiotemporal spike events has been only rarely investigated

(Grün et al., 2002a; Pipa & Grün, 2003; Gerstein, 2004; Louis, Borgelt, & Grün, 2010; Louis et al., 2010; Ventura et al., 2005), and in particular, which conclusions arise if such features of experimental spike trains are ignored. Figure 1 illustrates the influence of non-Poisson spike train structure (here modeled as renewal gamma processes) on the distribution of coincident spike events. The comparison of the distributions to the one of Poisson processes demonstrates that the shape of the coincidence distribution may be considerably affected by the spike train structure. Thus, assuming Poisson in the presence of non-Poisson processes would lead to incorrect estimations of the statistical significance of coincident spiking activity. This aspect will be rigorously evaluated in the first part of this letter. Two types of renewal processes (gamma and log-normal processes) considered as reasonable models for experimental spike trains (Burns & Webb, 1976; Levine, 1991; Teich et al., 1997) are used for the investigation. Their ISI characteristic can be parameterized by the coefficient of variation (C_V) and thus can be varied from a bursty to a regular spike train structure. The influence of wrongly assumed spike train structure onto the distribution used for significance estimation will be shown by analytical and numerical methods.

Another approach increasingly used for the creation of surrogate data for significance evaluation of correlated spike trains is dithering (Date, Bienenstock, & Geman, 1998; Davies, Gerstein, & Baker, 2006; Gerstein, 2004; Hatsopoulos, Geman, Amarasingham, & Bienenstock, 2003; Shmiel et al. 2006). This procedure is also often called *jittering* (Kuhn, Aertsen, & Rotter, 2003), but we prefer to reserve the term *jitter* for the temporal imprecision in the original data and use *dithering* for the manipulation of the data (Grün, 2009). The method intentionally destroys existing spike correlation by a small displacement of the timing of each individual spike by a random amount. Therefore, the rate profiles stay almost unchanged. However, obviously this procedure interacts with the inter spike intervals of the original spike trains, and thus must lead to changes of the coincidence distribution. Although the efficiency of dithering was recently studied (Pazienti, Diesmann, & Grün, 2007; Pazienti, Maldonado, Diesmann, & Grün, 2008), there are no systematic investigations of the consequences of spike dithering on the significance evaluation of correlation. Here we will show first how the spike train structure interacts with dithering and, second, under which conditions the method may lead to false-positive results. Finally we discuss the results and methods to avoid false-positive results and incorrect data interpretation.

2 Spike Train Models

Although it is well known that spike trains are not Poissonian, this assumption is often used for simplicity for analytical and statistical purposes. Three main facts clearly indicate that biological spike trains have an autostructure that deviates from Poissonian processes. First, all neurons exhibit refractory periods after spike firing. This refractoriness makes short interspike
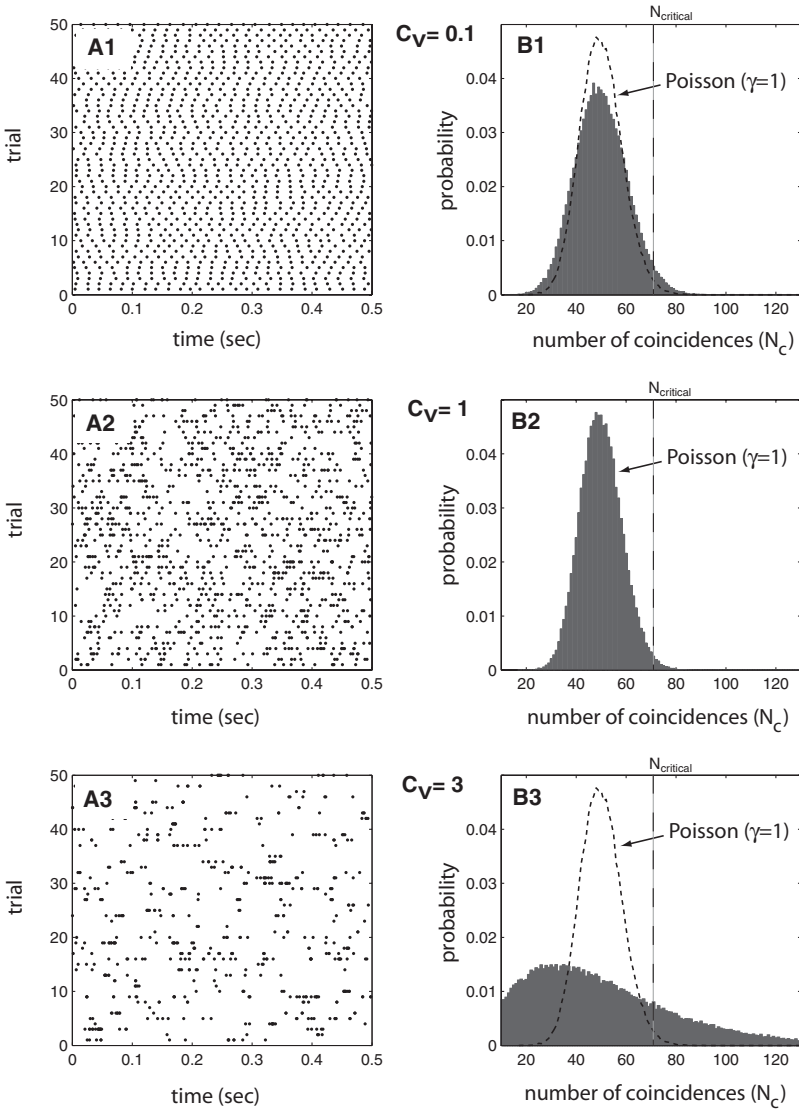
intervals on the order of several milliseconds unlikely to happen and is therefore incompatible with the exponentially decaying interspike interval distribution of a Poisson process (Cox & Lewis, 1966). Second, biological neurons can fire with a certain temporal structure that can be described in a first approximation as regular or bursty firing. In the latter case, neurons fire two or more spikes during short epochs, followed by longer episodes of

silence. And third, neuronal firing might not be described by renewal processes but exhibit higher-order dependencies of spike times that lay further back in the past (Nawrot et al., 2007). In this letter, we focus on the first two aspects and assume that the neuronal firing can be described by renewal processes. We study the impact of the refractoriness, the burstiness, and the regularity of spike trains on the probability distribution of coincident firing.

To this end, we use two models of neuronal firing that are both renewal processes with two model parameters each: the gamma process and the lognormal process. Both processes allow us to model burstiness, regularity, and refractoriness for different parameter combinations, and both have been proposed as model descriptions for neuronal spike trains (Burns & Webb, 1976; Levine, 1991; Teich et al., 1997; Iyengar & Liao, 1997; Nawrot et al., 2007, 2008; Smith, 1954a, 1954b).

2.1 Gamma Process. A gamma process occurs naturally when an integrate-and-fire model is driven by a Poisson input (Gerstein & Mandelbrot, 1964). The gamma process is a renewal process and is therefore characterized only by the interspike interval (ISI) distribution ($p(t)$). The ISI distribution for a gamma process with a given constant spike rate is described by

$$p_\gamma(t) = t^{\gamma-1} \frac{(\gamma R)^\gamma \ e^{-\gamma Rt}}{\Gamma(\gamma)} \qquad \text{for } t > 0. \tag{2.1}$$

This distribution is characterized by two variables: the spike rate R and the shape parameter γ. The Poisson process is a special case of the gamma

---

Figure 1: (A1–A3) Raster plot for 50 trials of independent gamma processes with three different coefficients of variation of the inter spike interval distribution (A1, B1: $C_V = 0.1$; A2, B2: $C_V = 1$; A3, B3: $C_V = 3$). (B1–B3) Distribution of coincidence counts shared by pairs of mutually independent gamma processes of the same kind as shown in panel A. Coincidence counts are derived as the sum of the binwise products of the spikes counts per bin. Dashed curves in (B1 and B3) show the coincidence count distribution of B2, which equals the case of Poisson processes ($\gamma = 1$), as a reference curve. $N_{critical}$ shown in B1, B2, B3 indicates the critical number of coincidences that corresponds to a 1% significance level under the assumption that the underlying spike trains are Poissonian. Hence, any number of coincidences larger than or equal to $N_{critical}$ would be classified as significant. Coincidences were evaluated per trial based on a binned version (bin length: $\Delta t = 4\,\text{ms}$) of the original renewal process. Each distribution in panel B represents a sample from $T = 100,000$ trials of each 5 s length. The spike rate was chosen to be $R = 50\,\text{Hz}$. The false-positive rate in B1 and B3 were increased in relation to the test level by 3 and 22 times (3%, and 22%), respectively.

process for which $\gamma = 1$. Values of the shape parameter γ smaller than 1 make the distribution become hyperexponential, and short intervals are more likely to occur than for a Poisson process with the same rate. We use this parameter regime of a gamma process with a shape parameter smaller than 1 in order to model bursty spike trains. In contrast, for very large values of the shape parameter γ, the gamma distribution approaches a narrow normal distribution. Therefore, a gamma process with shape parameter $\gamma > 1$ is used to model regular firing.

To model gamma spike trains given a certain coefficient of variation C_V of the interspike interval distribution ($C_V = \sigma_t / \langle t \rangle$), we use the expected value of the interspike interval $\langle t \rangle = 1/R$ and the variance $\sigma_t^2 = 1/(\gamma R^2)$ to express the shape parameter γ by the coefficient of variation C_V:

$$\gamma = \frac{1}{C_V^2}. \tag{2.2}$$

2.2 Log-Normal Process. The log-normal process is a renewal process with log-normal distributed interspike intervals. Its interspike interval distribution ($p(t)_{log-normal}$) is defined by

$$p(t)_{log-normal} = \frac{1}{k\sqrt{2\pi}} \frac{\exp\left(-\frac{(\ln(t)-a)^2}{2k^2}\right)}{t}. \tag{2.3}$$

Compared to the ISI distribution of a gamma process, the log-normal ISI distribution is more heavy tailed for the same C_V and very short intervals, even for high C_V, are unlikely to happen. The moments of the log-normal distribution are given by

$$\langle t^n \rangle = \int_0^{+\infty} t^n p(t)\, dt = e^{na + \frac{n^2 k^2}{2}}. \tag{2.4}$$

To model spike trains given an expected spike rate, R, and coefficient of variation, C_V, we can express the parameters a and k as

$$a = -\ln R - \frac{1}{2} \ln\left(C_V^2 + 1\right) \tag{2.5}$$

and

$$k = \sqrt{\ln\left(C_V^2 + 1\right)}. \tag{2.6}$$

3 Coincidence Count Distribution

In this section, we derive and discuss the impact of the interspike interval distribution on the shape of coincidence count distributions. To stress the importance of this interplay we first give a few examples in order to demonstrate that the impact of the detailed interspike interval distribution on the coincidence count distribution can be important. The first example we look at is the comparison of different renewal processes that look identical concerning two features that are frequently used to characterize biological spike trains: the C_V of the interspike interval distribution and the Fano factor FF_s of the spike count distributions. As a second example, we show that dithering of individual spikes can alter the coincidence count distribution for different renewal processes characterized by the same C_V in very different ways.

Following these examples, we present analytical expressions and a rigorous discussion of the mean and the variance of the coincidence count distribution for a frequently used model of biological spike trains, the gamma process in the case of integer shape parameters. We then complement this analytical derivation by numerical estimations of the mean and the variance for gamma processes with noninteger shape parameters as well as with a second kind of renewal process with log-normal-distributed interspike intervals.

3.1 Coincidences. Given two parallel spike train processes, we define a coincidence based on binned versions of the original processes. The binned spike trains are obtained by segmenting the time axis into exclusive bins, each of length Δt, and counting the exact number of spikes n_k per bin k (no clipping; clipping reduces any number of spikes larger than 1 to 1; see Grün, Diesmann, & Aertsen, 2002b). The number of coincidences in bin k shared by the two corresponding simultaneous bins of neurons 1 and 2 is then defined by $N_c^k = n_k^1 n_k^2$.

3.1.1 Examples of Coincidence Count Distributions for Gamma and Log-Normal Processes. As a first example of the importance of the interspike interval distribution on the coincidence count distribution, we show in Figures 2 and 3 the coincidence count distributions for gamma and log-normal processes for the case of four different C_Vs but equal spike rate R and bin widths Δt. Figures 2B1 and 3B1 show the coincidence count distribution for a gamma and log-normal process, respectively, in case of very regular spiking activity, yielding a C_V of 0.1. In contrast, panel B4 in both figures shows the coincidence count distribution for a C_V of 1.5. Note that the nature of the log-normal distribution makes very short intervals unlikely, even for C_V values larger than 1, while short intervals are likely for the same C_V in the case of a gamma process.
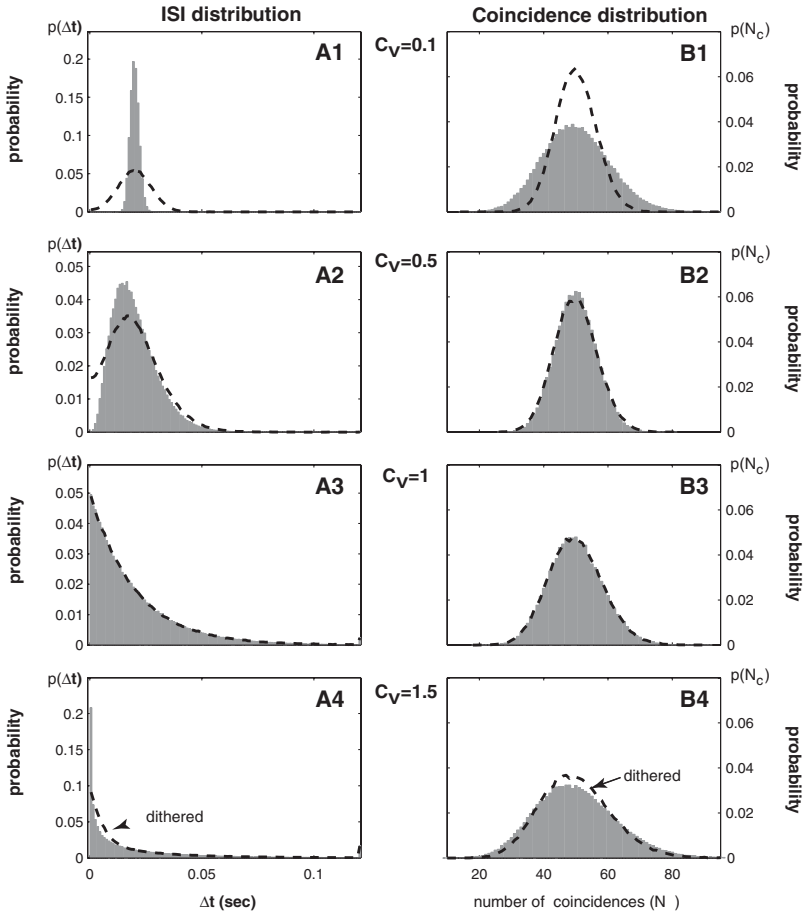
Figure 2: (A1–A4) Interspike interval distribution of gamma processes. The solid distribution is the ISI distribution of the original gamma process, while the dashed curve indicates the ISI distribution after individual spikes of the original gamma process were dithered by a random displacement normally distributed with zero mean and a standard deviation of $\sigma_d = 5$ ms. (B1–B4) Count distribution $p(\Delta t)$ of coincidences between two mutually independent gamma processes of the same kind as shown in A1–A4. Coincidences were evaluated per trial based on a binned version (bin length: $\Delta t = 4$ ms) of the original renewal processes. The coincidence count distribution is shown for two variations: a binned version of the original gamma processes (gray filled) and a second process, where spikes of the original Gamma processes have been dithered first and then binned (dashed). Each distribution in panels A and B represents a sample from $T = 100,000$ trials, each of 5 s length. The spike rate was chosen to be $R = 50$ Hz. Different rows indicate different model C_Vs (A1, B1: $C_V = 0.1$; A2, B2: $C_V = 0.5$; A3, B3: $C_V = 1$; A4, B4: $C_V = 1.5$).
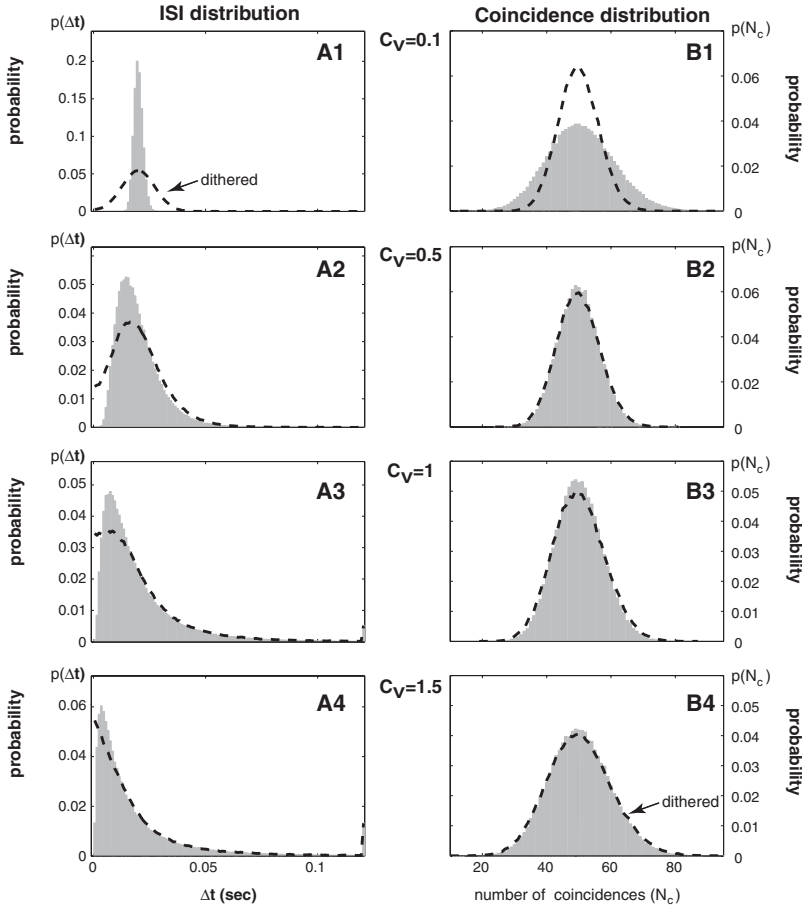
Figure 3: Same as shown in Figure 2, but for a log-normal interspike interval distributed renewal process. (A1–A4) ISI distribution of log-normal processes (shaded gray area: ISI distribution of the original log-normal process; dashed: after dithering). (B1–B4) Count distribution $p(\Delta t)$ of coincidences between two mutually independent log-normal processes of the same kind as shown in A1–A4. The coincidence count distribution for the original log-normal processes (binned) is shown in gray (filled) and for dithered spikes before binning was applied (dashed). Same parameters as in Figure 2.

That difference in the likelihood of short ISIs makes the distribution of the coincidence counts much broader in the case of the gamma process than for the log-normal process (see Figures 4A, 5A3, and 5B3 for quantification of the broadening in terms of the Fano factor). This emphasizes that the

detailed structure, namely, the stronger burstiness for Gamma compared to log-normal processes, is responsible for making the coincidence distribution different even though the C_V and the FF_s of the spike counts are identical.

3.1.2 Example for the Effect of Dithering on the Coincidence Count Distribution. Another peculiarity occurs when individual spikes are dithered (Date et al., 1998; Davies et al., 2006; Gerstein, 2004; Hatsopoulos et al., 2003; Shmiel et al., 2006). This technique is often used for statistical purposes to derive surrogate data (e.g., to derive the probability of coincidence firing under the assumption that neurons fire independently). Dithering is defined by a random variation of the spike timing of individual spikes by a random offset, for example, drawn independently and identically distributed (i.i.d.) from a gaussian distribution with zero mean and variance σ_d^2 (Jones, Depireux, Simons, & Keller, 2004). Since the gamma process with $C_V = 1$ is actually a Poisson process, dithering affects neither the ISI distribution nor the coincidence count distribution, as shown in Figure 2B3.

However, although the C_V and the Fano factor of the spike count distribution are identical for both the Poisson and the log-normal distribution, dithering changes the shape of the coincidence count distribution for the log-normal process (see Figure 3B3) but not for the Poisson processes (see Figure 2B3). In contrast, we see the opposite effect for $C_V = 1.5$. Dithering changes the coincidence distribution in case of the gamma process, but it stays nearly unchanged for the log-normal process. These examples show that dithering changes the shape of the coincidence count distribution in a rather unpredictable way when the nature of the underlying process is unknown.

3.2 Fano Factor (FF_C) of Coincidence Count Distribution for Renewal Processes. After having presented examples that emphasize the necessity of a deeper understanding of the interplay between the nature of a renewal process and the coincidence count distribution, we now give a rigorous analytical description of the mean and the variance of the coincidence count distribution of a gamma process with integer shape parameter $\gamma \in \mathbb{N}$.

To this end, we first derive the expected number of coincidences. If n_k^i is the number of spikes from neuron i in bin k, the number of coincidences, N_c, counting over bins $k = 0$ to $K - 1$ is

$$N_c = \sum_{k=0}^{K-1} n_k^1 n_k^2. \tag{3.1}$$

The average number of coincidences, $\langle N_c \rangle$, is given by

$$\langle N_c \rangle = \left\langle \sum_{k=0}^{K-1} n_k^1 n_k^2 \right\rangle = \sum_{k=0}^{K-1} \langle n_k^1 n_k^2 \rangle = K \langle n_k^1 n_k^2 \rangle. \tag{3.2}$$

If the spike times of the two neurons are generated by independent station-
ary renewal processes (in equilibrium), this is equal to

$$\langle N_c \rangle = K \langle n_k^1 \rangle \langle n_k^2 \rangle = K R_1 R_2 (\Delta t)^2, \tag{3.3}$$

where Δt is the bin width and R_i the rate of neuron i. This result demon-
strates that the expected number of coincidences is independent of the
nature of the renewal process.

Next, we derive the variance of the coincidence count distribution and
use it to calculate the Fano factor FF_c. The mean square of the spike count,
$\langle N_c^2 \rangle$, satisfies

$$\langle N_c^2 \rangle = \left\langle \left(\sum_{k=0}^{K-1} n_k^1 n_k^2 \right)^2 \right\rangle$$

$$= \sum_{k=0}^{K-1} \sum_{l=0}^{K-1} \langle n_k^1 n_l^1 n_k^2 n_l^2 \rangle$$

$$= \sum_{k=0}^{K-1} \sum_{l=0}^{K-1} \langle n_k^1 n_l^1 \rangle \langle n_k^2 n_l^2 \rangle$$

$$= \sum_{k=0}^{K-1} \sum_{l=0}^{K-1} A_{k-l}^1 A_{k-l}^2. \tag{3.4}$$

Here we have used the independence of the renewal processes to write
$\langle n_k^1 n_l^1 n_k^2 n_l^2 \rangle = \langle n_k^1 n_l^1 \rangle \langle n_k^2 n_l^2 \rangle$, and A_k^i is the autocorrelation for the binned spike
train of neuron i, $A_k^i = \langle n_l^i n_{l+k}^i \rangle_l$. The variance in the number of coincidences,
$\sigma^2(N_c)$, is

$$\sigma^2(N_c) = \sum_{k=0}^{K-1} \sum_{l=0}^{K-1} \left[A_{k-l}^1 A_{k-l}^2 - (R_1 R_2)^2 (\Delta t)^4 \right]. \tag{3.5}$$

Using $k_+ = k + l$ and $k_- = k - l$, this can be written as

$$\sigma^2(N_c) = \sum_{k_- = -K+1}^{K-1} \sum_{k_+ = |k_-|}^{2K-2-|k_-|} {}^* \left| A_{k_-}^1 A_{k_-}^2 - (R_1 R_2)^2 (\Delta t)^4 \right., \tag{3.6}$$

where we have used $\sum_{k_+ = |k_-|}^{2K-2-|k_-|} |^*$ to denote that in the sum over k_+, only
every second term should be taken. The reason for that restriction is that

the combination of $k_+ + k_- = 2k$ and $k_+ - k_- = 2l$ makes k_+ take only even values if k_- is even and k_+ take only odd values if k_- is odd.

Using this relation, we obtain $\sum_{k_+=|k_-|}^{2K-2-|k_-|} |^* = K - |k_-|$, so that the variance can be written as

$$\sigma^2(N_c) = \sum_{k_-=-K+1}^{K-1} (K - |k_-|) \left[A_{k_-}^1 A_{k_-}^2 - (R_1 R_2)^2 (\Delta t)^4 \right]. \qquad (3.7)$$

Using this and equation 3.3, the Fano factor of the coincidence count distribution, FF_c, can be written as

$$FF_c = \frac{\sigma^2(N_c)}{\langle N_c \rangle} = \frac{1}{R_1 R_2 (\Delta t)^2} \sum_{k=-K+1}^{K-1} \left(1 - \frac{|k|}{K} \right) \left[A_k^1 A_k^2 - (R_1 R_2)^2 (\Delta t)^4 \right]. \qquad (3.8)$$

Next we take the limit $K \to \infty$ and use the fact that as $|k|$ approaches infinity ($|k| \to \infty$), A_k^i approaches $(R_i \Delta t)^2$ exponentially. Therefore, $A_k^1 A_k^2 - (R_1 R_2)^2 (\Delta t)^4$ approaches 0 exponentially as $|k|$ increases.

As a result, the term that involves $|k|/K$ becomes negligible as K becomes large. In consequence, as K increases, the Fano factor approaches

$$FF_c = \frac{1}{R_1 R_2 (\Delta t)^2} \sum_{k=-\infty}^{\infty} \left[A_k^1 A_k^2 - (R_1 R_2)^2 (\Delta t)^4 \right]. \qquad (3.9)$$

Using the symmetry of the autocorrelation, this can also be written as

$$FF_c = \frac{A_0^1 A_0^2 - (R_1 R_2)^2 (\Delta t)^4}{R_1 R_2 (\Delta t)^2} + 2 \sum_{1}^{\infty} \frac{A_k^1 A_k^2 - (R_1 R_2)^2 (\Delta t)^4}{R_1 R_2 (\Delta t)^2}. \qquad (3.10)$$

Note that the analytical expression described so far for the Fano factor, equation 3.10 holds for any renewal process as well as any stationary non-renewal point process for which the autocorrelation approaches $R^2(\Delta t)^2$ sufficiently quickly.

3.3 Analytical Derivation of FF_c for Poisson Processes. In general there is no way to arrive at an analytical expression for equation 3.10 from the interspike interval distribution of a given spike train i, $p_i(t)$. However, for the simplest case of a renewal process, namely, the Poisson process ($p_i(t) = R_i \exp(-R_i t)$), the Fano factor becomes a very simple expression. To derive the autocorrelation of the Poisson process, we use $A_k^i = R_i \Delta t \delta_k + (R_i \Delta t)^2$,

where δ_k is the Kronecker delta. δ_k takes the value of 1 for $k = 0$ and the value of 0 otherwise. This simplifies equation 3.10 to

$$FF_c = 1 + (R_1 + R_2)\Delta t. \tag{3.11}$$

Note that FF_c is larger than 1 and grows with increasing spike rates and bin width. The reason is that we counted the number of coincidences as the product of the number of spikes of simultaneous bins (see equation 3.1).

Mostly for simplification, an alternative way of counting coincidences has been proposed that requires that the spike trains be binary sequences. In this case, the number of coincidences per bin can be either 0 or 1 (clipping). Note also that in this case, the Fano factor FF_c^{clip} does not equal 1. In fact, FF_c^{clip} is smaller than 1 in the case of underlying Poisson processes.

3.4 Analytical Derivation of FF_c for Gamma Processes. After having derived the Fano factor FF_c for Poisson processes, we derive a closed analytical expression of FF_c for gamma processes.

In appendix B we show that for a γth-order gamma process with integer γ and rate R, the autocorrelation A_k satisfies

$$A_0 = \frac{R\Delta t}{\gamma} + (R\Delta t)^2 - 2\sum_{l=1}^{\gamma-1} B_l \quad \text{with } \gamma \in \mathbb{N} \tag{3.12}$$

and, for $k \neq 0$,

$$A_k = (R\Delta t)^2 + \sum_{l=1}^{\gamma-1} B_l(1 - Z_l)[Z_l]^{|k|-1} \tag{3.13}$$

where, using $x_\gamma^l = \exp(2\pi \frac{l}{\gamma}i)$, Z_l satisfies

$$Z_l = \exp[-(1 - x_\gamma^l)\gamma R\Delta t], \tag{3.14}$$

while

$$B_l = \frac{x_\gamma^l}{\gamma^2(1 - x_\gamma^l)^2}(1 - Z_l). \tag{3.15}$$

Inserting this into equation 3.10 and using $\sum_{k=1}^{\infty} z^k = z/(1 - z)$ for $|z| < 1$, we obtain, after some algebra, the following value for the Fano factor of the number of coincidences for two independent spike trains generated by

gamma processes with rates R_i and shape parameter γ_i,

$$
FF_c = \frac{1}{\gamma_1 \gamma_2} + \frac{R_1 \Delta t}{\gamma_2} + \frac{R_2 \Delta t}{\gamma_1} - \frac{2}{\gamma_1 R_2 \Delta t} \sum_{l=1}^{\gamma_2 - 1} B_l^2 - \frac{2}{\gamma_2 R_1 \Delta t} \sum_{k=1}^{\gamma_1 - 1} B_k^1
$$

$$
+ \frac{4}{R_1 R_2 (\Delta t)^2} \sum_{k=1}^{\gamma_1 - 1} \sum_{l=1}^{\gamma_2 - 1} B_k^1 B_l^2 \left(1 + \frac{1}{2} \frac{(1 - Z_k^1)(1 - Z_l^2)}{1 - Z_k^1 Z_l^2} \right), \qquad (3.16)
$$

where Z_l^i and B_l^i are determined by equations 3.14 and 3.15 using the parameters R_i and γ_i.

Hence, equation 3.16 is a closed analytical expression for the Fano factor FF_c of the coincidence count distribution of two mutually independent gamma processes with integer shape factors in case coincidences are counted by the product of spike counts per bin as defined in equation 3.1.

Using equation 3.16, we then studied the functional dependencies of FF_c as a function of, the shape parameter, different rates for the two spike trains considered simultaneously, and, the product of the bin width and the spike rate $R\Delta t$ (see Figure 4).

In Figure 4A we plot FF_c as a function of the C_V for four variations of the product of the spike rate and the bin width $R\Delta t$ for two processes with identical rate $R = R_1 = R_2$ and identical shape factors $\gamma = \gamma_1 = \gamma_2$. It demonstrates that the value of FF_c changes nonmonotonically with increasing values of C_V. For a low order of γ, FF_c decreases with increasing shape parameter, while FF_c increases with γ for larger values of the shape parameter. Moreover, although FF_c is below 1 for all four variations of $R\Delta t$ for an intermediate range of the C_V, it is larger than 1 for low and high values of the C_V.

As a second variation, Figure 4B, we used equation 3.16 to study changes of the Fano factor FF_c as a function of the C_V for the case that the rates of processes 1 and 2 are differing but have the same shape factors $\gamma = \gamma_1 = \gamma_2$. The bin width is chosen such that $R\Delta t = 0.2$. We quantify the difference in rate by $\Delta R/R$ with $R_1 = R + \Delta R$ and $R_2 = R - \Delta R$. For $\gamma = 1$, the Fano factor is $FF_c = 1 + (R_1 + R_2)\Delta t = 1.4$ and does not depend on ΔR, such that we reproduce the results from Figure 4A. For small values of γ, the dependence on ΔR is weak, but for large γ, there is a strong dependence. However, this dependence is not monotonic either.

For small differences of $\Delta R/R$ that are larger than $\Delta R/R = 0.1$, the qualitative behavior for small values of C_V is quite different and stays below 1, while the difference across differences of $\Delta R/R$ for larger values of the C_V disappears.

In Figure 4C we study FF_c as a function of the difference in rate $\Delta R/R$ for five different shape parameters and $R\Delta t = 0.2$. Again the plot demonstrates that the behavior is not linear or trivial. With increasing shape parameter,
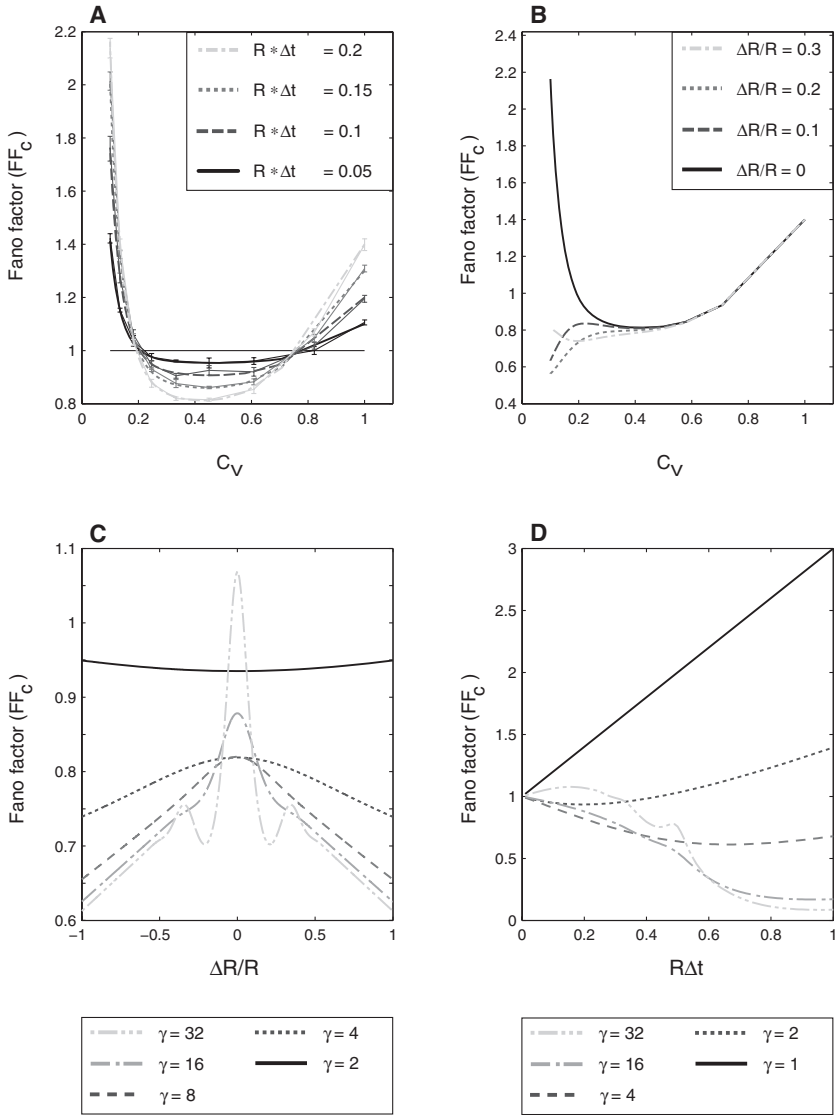
Figure 4: Analytically determined Fano factor FF_c. (A) FF_c as a function of the C_V for four different products $R\Delta t$. (B) As in panel A, FF_c as a function of the C_V, but for for two neurons with different rate $R_1 = R + \Delta R$ and $R_2 = R - \Delta R$ and a bin width Δt so that $R\Delta t = 0.2$. (C) FF_C as a function of $\Delta R/R$ for the order $\gamma = 2, 4, 8, 16, 32$ for the same bin width. (D) FF_C plotted against the product $R\Delta t$ for gamma processes with $\gamma = 1, 2, 4, 16, 32$.

the mapping becomes more complex. While it is monotonic as a function of the absolute value of $\Delta R/R$ for shape factors $\gamma = 2, 4, 8, 16$, the relation becomes nonmonotonic for shape parameter $\gamma = 32$. For larger γ, the FF_c has a maximum for $\Delta R = 0$ and drops more rapidly with $|\Delta R|$ as γ is increased. However, for very large γ, there is a secondary peak for $\Delta R \approx 1/3$ for this value of ΔR, $R_1 = 2R_2$. Presumably for even larger γ, there is another peak when $R_1 = 3R_2$. This illustrates that the Fano factor of the coincidence counts can change quite unexpectedly and strongly even for very small differences in the spike rates of two independent processes if the gamma processes becomes very regular.

As a last variation (see Figure 4D), we study FF_c as a function of the $R\Delta t$ for five variations of the shape factor γ. Again the complexity of the behavior increases with increasing shape factor. For a Poisson process, FF_c grows linearly with the rate difference $R\Delta t$, while it is also nonmonotonic for shape factors $\gamma = 2, 4, 16, 32$.

This set of results demonstrates that the Fano factor FF_c of the coincidence count distribution depends in a complex and nonintuitive way on all three parameters: the shape factor γ and the C_V, the product of the spike rate and the bin width $R\Delta t$, and the difference between the spike rates of two independent gamma processes.

The fact that even small changes of single parameters that are each in a biological plausible range can alter the Fano factor quite heavily and emphasize that a statistical inference on coincident firing may fail in case that it is based on the assumption that neuronal firing can be approximated by Poissonian processes. We find that if the C_V of the processes is approximately smaller than 0.2 or larger than 0.7, the significance would be overestimated, and for values in between, it would be underestimated (see Figure 4A). The picture changes if the firing rates of the two processes differ. Then the significance tends to be underestimated for small CVs (see Figure 4B and 4C). The underestimation is stronger if rate differences are larger (see Figure 4D).

**3.5 Numerical Estimation of the Coincidence Count Distribution.** Next, we complement the analytical results from the last section with numerical estimations for the gamma processes with noninteger order parameter and use log-normal processes as a second kind of renewal processes. As for the analytical derivation of the Fano factor FF_c for the coincidence count distribution, we choose the coefficient of variation (C_V) of the ISI distribution for the parameterization of both processes (see equations 2.2 and 2.6). We first checked the correspondence between the analytically predicted model C_V and the numerical estimation for the gamma and log-normal process (see Figures 5A1 and 5B1). For all tested parameter combinations, the numerical estimations of C_V corresponded to the analytically predicted values.

In a further step, we study the effect of dithering of individual spikes (i.i.d., gaussian, zero mean, and 5 ms standard deviation) of gamma and log-normal processes on the C_V of the resulting processes (see Figures 5A2 and 5B2). Dither widths as small as 5 ms change the C_V of the original process quite strongly and increase the C_V. This is because processes with small values of C_V have many pairs of spikes that occur in short intervals and can be characterized as bursty. This bursty activity is destroyed for even small amounts of dithering, since the short timescale of the dithering is comparable to the timescale of the bursts. For an original C_V of about 1, there is no obvious change, but for original C_V larger than 1, there is a tendency for resulting C_Vs to be smaller than 1. Intuitively that can be explained by the fact that dithering makes the interspike interval distribution of any kind of spiking activity more Poisson.

To estimate FF_C for noninteger gamma processes with shape factors γ ranging from 0.$\bar{4}$ to 100 (C_V from 0.1 to 1.5), as well as renewal processes with log-normal distributed ISIs for values of C_V between 0.1 to 1.5, we used Monte Carlo estimations (see Figures 5A3 and 5B3; for details regarding the numerical procedure, see appendix C). The numerical results of the gamma process correspond to the analytically predicted values (compare Figure 4A). For shape parameters smaller than 1, for which we do not have analytical predictions, the value FF_c grows with increasing C_V and increases of the product $R\Delta t$. The qualitative behavior of changes of FF_c for a log-normal process as a function of the C_V are comparable to the changes in the case of a gamma process. Both processes exhibit nonlinear and nonmonotonic changes of FF_C as a function of C_V. Moreover, both processes exhibit a low FF_C for intermediate values of C_V, while values of FF_C are large for very low and high values of C_V.

In general, changes of FF_c are more pronounced for larger values of the product $R\Delta t$. This is true for both kinds of processes. However, despite the qualitatively identical behavior, changes for larger values C_V are up to two times stronger for log-normal processes than for gamma processes.

3.6 Comparison of the Full Distributions. To compare the full shape of the distribution of coincidence counts we use quantile-quantile (QQ) plots. We first compare the distribution for gamma (see Figure 6A1–6A3) and log-normal processes (see Figure 6B1–6B3) with the distribution for Poisson processes, for the case that all three types of processes have identical spike rates (R = 50 Hz). Differences between distributions resulting from gamma and log-normal processes as compared to Poisson processes are particularly obvious in the tails of the distributions. Because the average coincidence count is unaffected by the shape of the ISI distribution, the medians of the distributions are almost the same (QQ plots cut the diagonal close to 0.5). Large and small values of C_V, deviating from $C_V = 1$, make the coincidence count distributions of the gamma and log-normal processes more heavily tailed than the distribution resulting from Poisson processes, whereas for
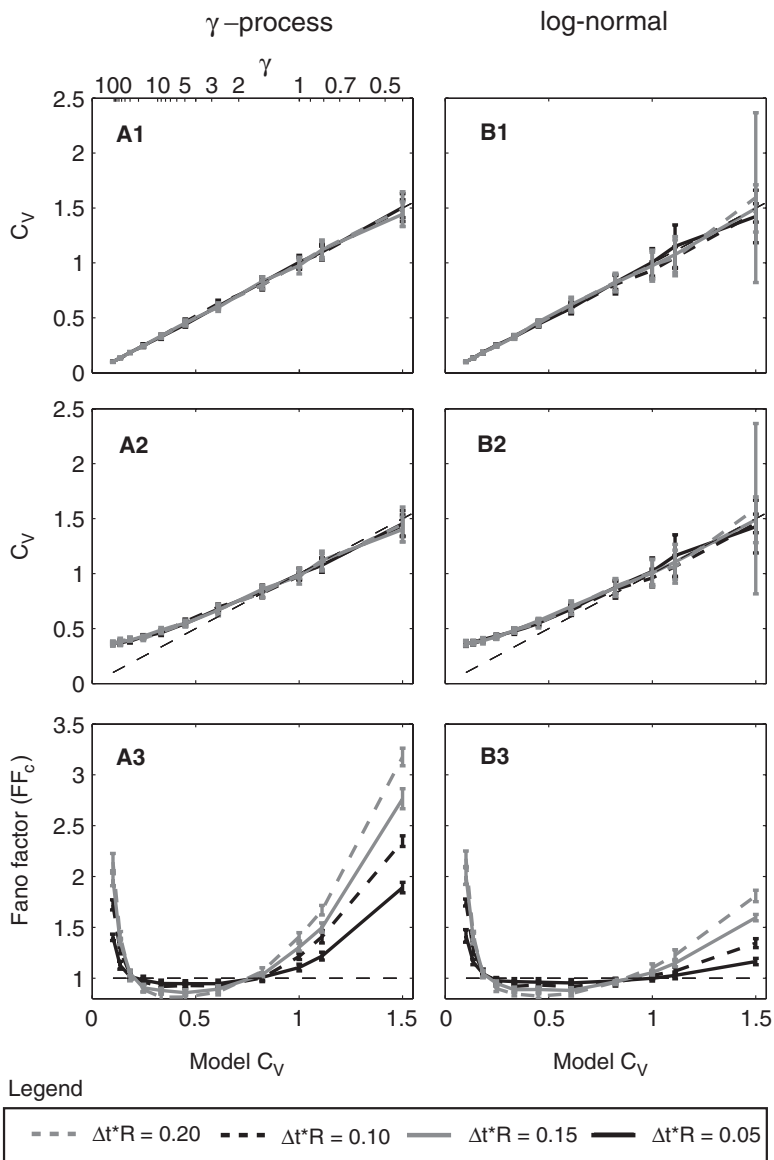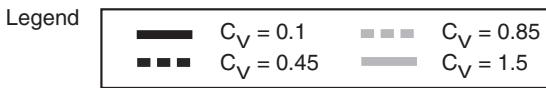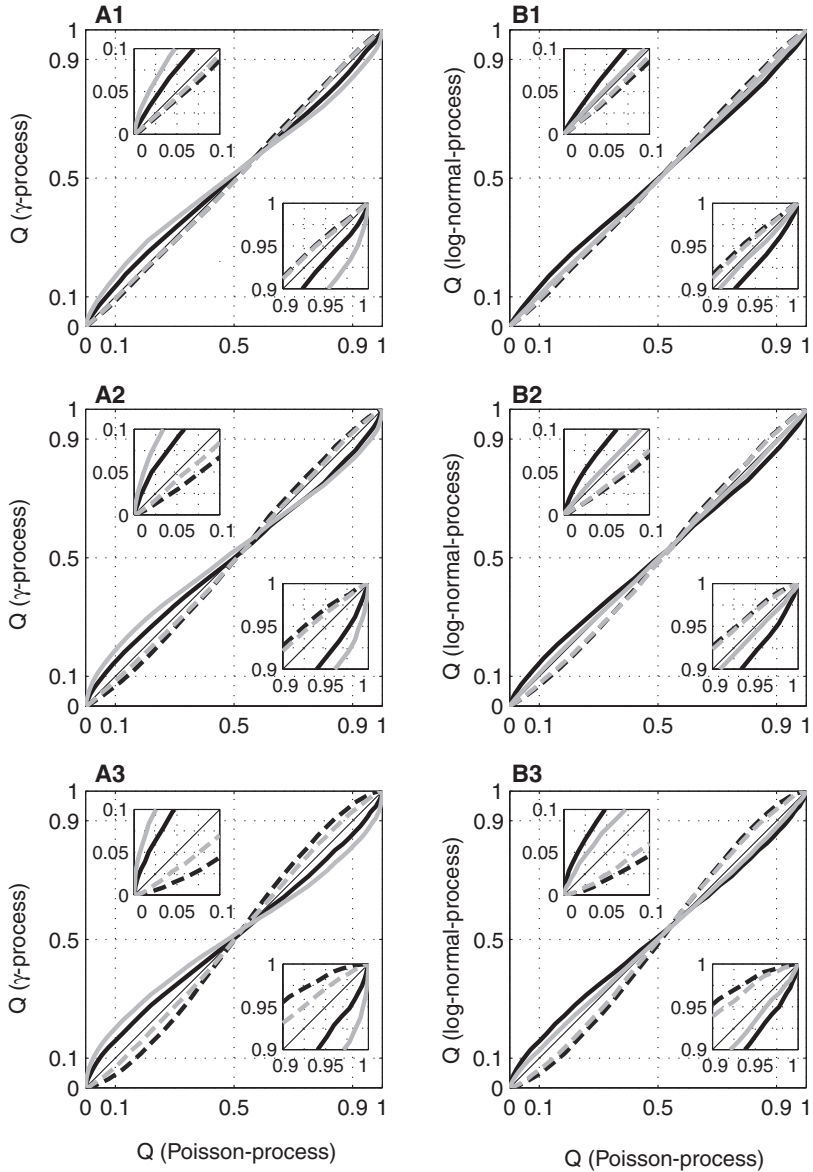
intermediate values of the C_V, their tails are less pronounced. The fact that these differences are especially pronounced in the tails implies strong consequences for hypothesis testing. To illustrate that, we added two insets for each QQ plot showing the first 10% from 0 to 0.1 corresponding to the left tail of the distribution (see the insets above the diagonals in Figure 6) and

the last 10% from 0.9 to 1 corresponding to the right tail of the distribution (insets below the diagonal in Figure 6).

For the left tail of the distribution, any curve above the diagonal indicates an increased false-positive level if the test statistics is based on the assumption that spike trains follow Poissonian firing. In contrast, any curve below the diagonal indicates a reduced number of false positives and therefore a conservative hypothesis test. The actual number of false positives in comparison to the given the test level (values along the x-axis) is equal to the value of the QQ curve (y-axis) at the given test level (x-axis). In the case of the right tail of the distribution (insets below the diagonal showing values ranging from 0.9 to 1), this relation is the opposite. Here, any curve below the diagonal indicates an increased level of false positives. For this case, the actual number of false positives, given the assumption of Poissonian firing, is equal to 1 minus the value at which the curve intersects a given value of the x-axis that equals the assumed test level. Note that the interpretation of false positives occurring at the different tails of the distribution would be interpreted differently. While false positives in the left tail of the distribution would be interpreted as an overestimation of lacking coincidences, they would be interpreted as an overestimation of excess synchrony at the right tail. Typically of interest are tests showing excess synchrony.

Differences between the distributions can be quite dramatic, such that the number of false positives can be considerably increased (see Figures 6A3 and B3) for large bin width, as well as for large values of the C_V. Qualitatively, changes for both types of processes, the gamma and log-normal, compared to Poisson are very similar. Quantitative differences are most pronounced in the tails, where differences in comparison to distributions generated by Poisson processes are generally strong.

Figure 5: Two different renewal processes are underlying results in A and B. (A) Gamma process with an interspike interval distribution following a gamma distribution. (B) Log-normal process following a log-normal distribution. (A1, B1) Estimated C_V on the y-axis as a function of the analytically predicted C_V. (A2, B2) Same as in (A1, B1), but individual spikes were dithered by a random time interval normally distributed with zero mean and a standard deviation of 5 ms. (A3, B3) Fano factor of the coincidence count distribution as a function of the model C_V. Coincidences were evaluated based on a binned version (bin length for black solid: $\Delta t = 1$ ms, black dashed: $\Delta t = 2$ ms, gray solid: $\Delta t = 3$ ms, grey dashed: $\Delta t = 4$ ms) of the original renewal process used in A1, A2, B1, and B2. Both process types (gamma and log normal) were parameterized by the product of the bin length Δt in units of s and the firing rate R in units of Hz (see legend). Each estimation of the C_V or Fano factor was based on $T = 2000$ trials of each 5 s length. The spike rate was $R = 50$ Hz. Error bars indicate one standard deviation.

Legend
- $C_V = 0.1$ (solid black)
- $C_V = 0.45$ (dashed black)
- $C_V = 0.85$ (dashed gray)
- $C_V = 1.5$ (solid gray)

4 Influence of Dithering on Coincidence Distribution

4.1 Analytical Approach for Gamma Processes. As we have shown, the Fano factor for the number of coincidences FF_c depends on the autocorrelations of the spikes trains of the two neurons, $A_k^{(i)}$. The autocorrelation of the spike trains after dithering is applied will be different from the autocorrelation of the undithered spike trains. Hence, dithering will change the shape of the distribution, and thus the Fano factor of the coincidence count.

In general, it is not possible to analytically derive the Fano factor of the coincidences after dithering. However, it is instructive to consider the extreme with an extremely large width of the dithering kernel. In this case, the autocorrelation becomes flat except for the peak at zero delay. Nevertheless, the process is not Poissonian, since dithering does not change the spike count distribution for the two processes.

To calculate the Fano factor of the coincidence count distribution, consider a case in which the neurons fire N_1 and N_2 spikes, respectively. With this extreme dithering, each spike has an equal probability of occurring in any of the bins, and the bin in which it occurs is independent from that of the other spikes. Therefore, the joint probability of having $\tilde{n}_k^{(i)}$ spike in bin k is

$$P_i\big(\tilde{n}_0^{(i)}, \tilde{n}_1^{(i)}, \ldots, \tilde{n}_{K-1}^{(i)}\big) = \frac{N_i!}{\tilde{n}_0^{(i)}!\tilde{n}_1^{(i)}!\cdots\tilde{n}_{K-1}^{(i)}!} \prod_{j=0}^{K-1} \left(\frac{1}{K}\right)^{\tilde{n}_j^{(i)}}. \tag{4.1}$$

The average number of coincidences in these dithered spike trains is

$$\langle N_c | N_1, N_2 \rangle = \sum_{k=0}^{K-1} \langle \tilde{n}_k^{(1)} \rangle \langle \tilde{n}_k^{(2)} \rangle$$

$$= K \langle \tilde{n}_k^{(1)} \rangle \langle \tilde{n}_k^{(2)} \rangle. \tag{4.2}$$

Figure 6: Quantile-quantile (QQ) plots describing the relation between two coincidence count distributions based on two different kinds of renewal processes. Each distribution represents a sample from $T = 10{,}000$ trials of each 5 s length. Each QQ plot shows the variation of four different model C_V values ($C_V = 0.1$, 0.45, 0.85, 1.5). (A1–A3) The Y-axis shows the quantile of the coincidence count distribution Q (gamma process) based on two mutually independent gamma processes, while the x-axis shows the quantile Q (Poisson process) for two mutually independent *Poisson* processes. For both the Q (gamma process) and the Q (*Poisson* process), the spike rate was chosen to be $R = 50$ Hz. Coincidences were evaluated per trial based on a binned version (bin length Δt) of both original renewal processes. (B1–B3) Same as shown in A1 to A3 but based on *log-normal* processes instead of gamma processes. Parameters for B1 to B3 are the same parameters as in A1 to A3. Different rows indicate different bin length Δt (A1, B1: $\Delta t = 1$ ms; A2, B2: $\Delta t = 2$ ms; A3, B3: $\Delta t = 4$ ms).

where $\langle \tilde{n}_k^{(i)} \rangle$, the average number of spikes in a bin, is the total number of spikes, N_i, divided by the total number of bins, K. Thus,

$$\langle N_c | N_1, N_2 \rangle = \frac{N_1 N_2}{K}. \tag{4.3}$$

The expected value of the square of the number of coincidences, given N_1 and N_2, satisfies

$$\langle N_c^2 | N_1, N_2 \rangle = \sum_{k=0}^{K-1} \sum_{l=0}^{K-1} \langle \tilde{n}_k^{(1)} \tilde{n}_l^{(1)} \rangle \langle \tilde{n}_k^{(2)} \tilde{n}_l^{(2)} \rangle$$

$$= K(K-1) \langle \tilde{n}_k^{(1)} \tilde{n}_l^{(1)} \rangle \langle \tilde{n}_k^{(2)} \tilde{n}_l^{(2)} \rangle + K \langle (\tilde{n}_k^{(1)})^2 \rangle \langle (\tilde{n}_k^{(2)})^2 \rangle. \tag{4.4}$$

Here $\langle \tilde{n}_k^{(i)} \tilde{n}_l^{(i)} \rangle$ is the expected value of the product of the number of spikes in two different bins, while $\langle (\tilde{n}_k^{(i)})^2 \rangle$ is the expected value of the square of the number of spikes in a bin. Using equation 4.1 for the probability distribution for the binned spike train, it is straightforward to show that

$$\langle \tilde{n}_k^{(i)} \tilde{n}_l^{(i)} \rangle = \frac{N_i(N_i - 1)}{K^2} \tag{4.5}$$

and

$$\langle (\tilde{n}_k^{(i)})^2 \rangle = \frac{N_i(N_i - 1)}{K^2} + \frac{N_i}{K}. \tag{4.6}$$

Using this, we obtain, after some algebra, for $\langle N_c^2 | N_1, N_2 \rangle$

$$\langle N_c^2 | N_1, N_2 \rangle = \frac{N_1^2 N_2^2}{K^2} + \frac{N_1 N_2}{K} \left(1 - \frac{1}{K} \right). \tag{4.7}$$

To obtain the expected average $\langle N_c \rangle$ and mean square $\langle N_c^2 \rangle$ of the coincidences, we have to average these values over the distributions of the spike counts, N_1 and N_2:

$$\langle N_c \rangle = \left\langle \frac{N_1 N_2}{K} \right\rangle_{N_1, N_2}$$

$$= \frac{\langle N_1 \rangle \langle N_2 \rangle}{K} \tag{4.8}$$

and

$$\langle N_c^2 \rangle = \left\langle \frac{N_1^2 N_2^2}{K} + \frac{N_1 N_2}{K} \left(1 - \frac{1}{K}\right) \right\rangle_{N_1, N_2}$$

$$= \frac{(\langle N_1 \rangle^2 + \sigma^2(N_1))(\langle N_2 \rangle^2 + \sigma^2(N_2))}{K^2} + \frac{\langle N_1 \rangle \langle N_2 \rangle}{K} \left(1 - \frac{1}{K}\right). \quad (4.9)$$

Using this, we obtain for the Fano factor

$$FF_c \equiv \frac{\langle N_c^2 \rangle - \langle N_c \rangle^2}{\langle N_c \rangle}$$

$$= 1 + \frac{\langle N_1 \rangle}{K} \frac{\sigma(N_2)}{\langle N_2 \rangle} + \frac{\langle N_2 \rangle}{K} \frac{\sigma(N_1)}{\langle N_1 \rangle} + \frac{1}{K} \left(\frac{\sigma(N_1)}{\langle N_1 \rangle} \frac{\sigma(N_2)}{\langle N_2 \rangle} - 1 \right). \quad (4.10)$$

The expected value for the spike counts $\langle N_i \rangle$ is given by $\langle N_i \rangle = R_i K \Delta t$, while $\sigma(N_i) \langle N_i \rangle$ is just FF_s^i, the Fano factor for the spike count for neuron i. Thus, for large K, we obtain for the FF_c of extremely dithered spike trains in the large K limit

$$FF_c = 1 + \left(R_1 \times FF_s^{(2)} + R_2 \times FF_s^{(1)} \right) \Delta t. \quad (4.11)$$

Note that in this derivation, we have not used the fact that spike trains are renewal processes. This result holds for any stationary process.

If the spikes are generated by a renewal process, $FF_s^i(i)$ satisfies, for large K, $FF_s^{(i)} = [C_V^{(i)}]^2$, where $C_V^{(i)}$ is the coefficient of variation for neuron i. Thus, in the large K limit, the Fano factor after extreme dithering approaches

$$FF_c = 1 + \left(R_1 [C_V^{(2)}]^2 + R_2 [C_V^{(1)}]^2 \right) \Delta t \quad (4.12)$$

for renewal processes. For smaller amounts of dithering, we cannot easily obtain the autocorrelation after dithering analytically, but it can be obtained numerically from the autocorrelation of the undithered spike train.

To do this, we write the autocorrelation $A(t)$ as

$$A(t) = R\delta(t) + \tilde{A}(t), \quad (4.13)$$

where $R\delta(t)$ describes the part of the autocorrelation due to the same spike, while $\tilde{A}(t)$ describes the probability density for having two different spikes a time t apart. Similarly, we can write the autocorrelation $A_d(t)$ of the dithered spike train as

$$A_d(t) = R_d \delta(t) + \tilde{A}_d(t), \quad (4.14)$$

where R_d is the firing rate of the dithered spike train and $\tilde{A}_d(t)$ the probability density of two spikes in the dithered spike train being t apart. Since dithering does not change the firing rate, $R_d = R$, while the probability of two different dithered spikes being a time t apart is just the probability that in the original spike train, the spikes where $t - t_1 + t_2$, averaged over the probability that the first of these is displaced by an amount t_1 and the second by t_2. Thus $\tilde{A}_d$ satisfies

$$\tilde{A}_d(t) = \int\int \tilde{A}(t + t_2 - t_1)\kappa(t_1)\kappa(t_2)\, dt_2 dt_1, \tag{4.15}$$

where $\kappa(t)$ is the probability that a spike is dithered by an amount t. If the kernel κ is a gaussian with standard deviation, this can be simplified to

$$\tilde{A}_d(t) = \int \tilde{A}(t + t_1) \exp\left(-\frac{t_1^2}{4\sigma_d^2}\right) \frac{dt_1}{2\sqrt{\pi}\sigma_d}. \tag{4.16}$$

It is straightforward to calculate this numerically, after which it is easy to obtain the autocorrelation for the binned spike trains using the approach outlined in appendix B.

The impact of dither on the Fano factor FF_c is very nonintuitive. Changes of FF_c are monotonic for small shape factors of the gamma process and nonmonotonic for large shape factors and can amount to up to 40% of relative changes. The strongest changes occur for dithering of the order of 0.1 to 1 times the average interspike interval (see Figure 7).

This is exactly the range that is used for significance estimations, since any smaller amount of dithering does not destroy coincidences and any larger dithering could change the profile of rate changes. This emphasizes that the actual p-value describing the likelihood that coincidence events are due to chance might depend on the amount of dithering, whereas the relation can be nonmonotonic.

4.2 Appropriateness of Dithering to Realize the Null Hypothesis of Independence. So far we have analytically described the impact of dithering on the Fano factor FF_c of gamma processes with the integer shape factor. Next, we supplement the analytical expressions of FF_c by Monte Carlo–based estimations of the full shape of the distribution of coincidence counts of undithered and dithered gamma and log-normal processes. In addition, we explore how far the use of dithering is appropriate as an implementation of the null hypothesis of independence in a significance test of spike coincidences. Thus, we use the distribution of coincidence counts derived from mutually independent and dithered gamma and log-normal processes as respective reference distributions and estimate the probability for significant outcomes of the original, undithered spike trains. By comparing the distributions from the undithered to the dithered coincidence count
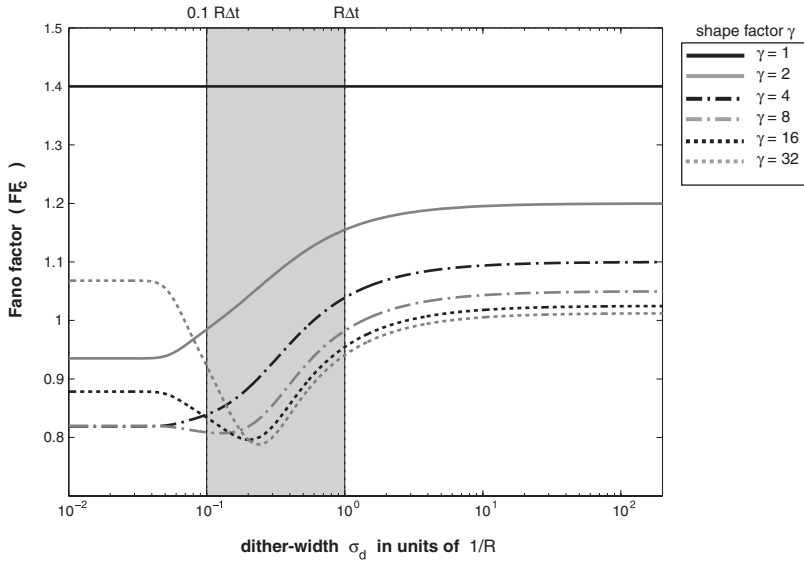
Figure 7: Analytically derived Fano factor of the coincidence count distribution for pairs of mutually independent gamma processes as a function of applied dither σ_d. To dither, the spike time of each individual spike time is changed by a random amount that was i.i.d. gaussian distributed with zero mean and a standard deviation σ_d. To achieve simplicity and uniformity, σ_d is expressed in units of the expected interspike interval $1/R$. The range of a typical jitter, from $0.1R\Delta t$ to $R\Delta t$, is indicated by a shaded area. Individual lines represent gamma processes with different shape factors γ ($\gamma = 1: C_V = 1/\gamma = 2: C_V = 0.7/\gamma = 4:$ $C_V = 0.5/\gamma = 8: C_V = 0.35/\gamma = 16: C_V = 0.25/\gamma = 32: C_V = 0.18$).

distributions, we derive an estimate of the probability of false-positive outcomes. This is done in the following way. We first determine the critical number of coincidences $N_{critical}$ from the coincidence count distribution of the dithered processes as the minimal count just becoming significant given the test level α such that $p(N \geq N_{critical}) =$ test level. Then we compute the probability of false positives of the corresponding undithered processes as $p(N^{undith} \geq N_{critical})$. Since these three numbers, N, N^{undith}, and $N_{critical}$, are integer numbers, we use a linear interpolation on the cumulative distribution of the reference distribution to derive an interpolated $N_{critical}$ to overcome variations in the effective significance level α occurring due to the discreteness of the coincidence count distribution. We use four different amounts of dithering ($\sigma_d = 5$ ms, 10 ms, 20 ms, and 40 ms) that are gaussian distributed with zero mean and a standard deviation of σ_d. The spike rate was 50 Hz and interspike intervals were gamma distributed in Figures 8A1 to A4 and log-normal distributed in Figures 8B1 to 8B4.

Legend

- - - σ_d = 40ms   —— σ_d = 20ms   - - - σ_d = 10ms   —— σ_d = 5 ms
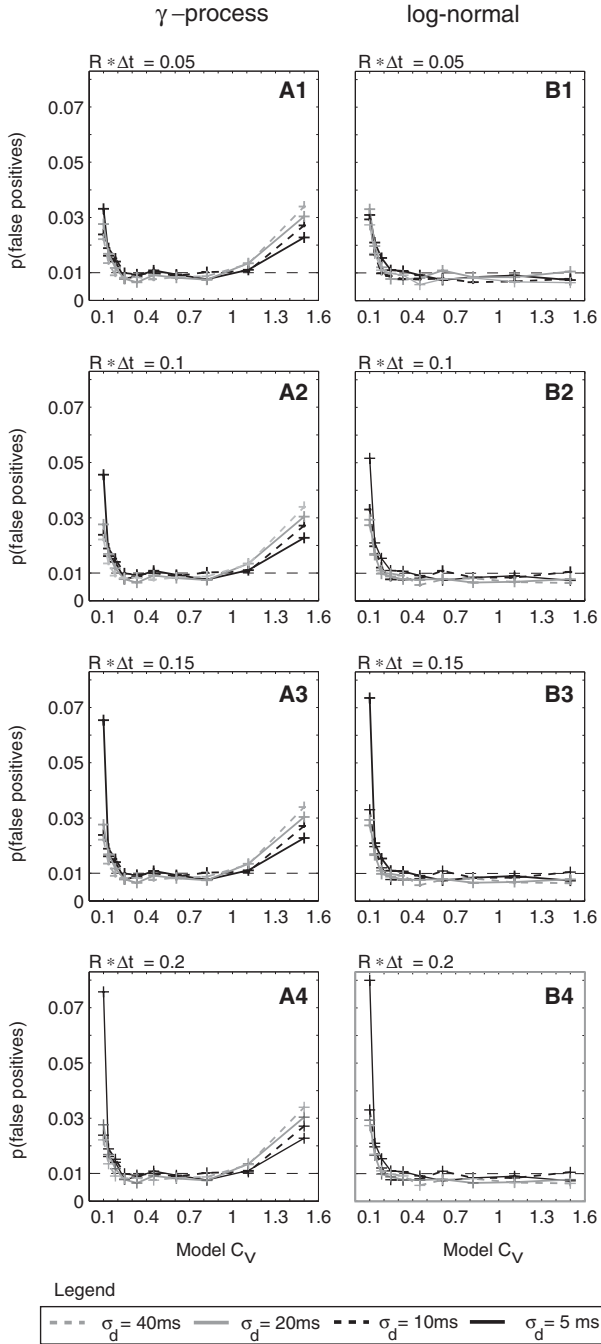
For low and intermediate values of the C_V, the qualitative and quantitative behavior of both process types is quite similar. Small values of the C_V lead to increases in the number of false positives up to seven times compared to the test level. Intermediate values of the C_V yield for both process types a level of false positives that is comparable to the test level. Only for high values of the C_V do the false positives behave differently for gamma and log-normal processes. While for gamma processes, the false positives increase, the false-positive rate is comparable to the test level in the case of log-normal processes. The reason is that the probability for small interspike intervals for log-normal processes and gamma processes is very different for larger C_V. In case of gamma processes, the distribution is hyperexponential, and short intervals are very likely, whereas for log-normal processes the probability for very short intervals is zero and very low for small ISIs. Since dithering destroys very short intervals more effectively than larger ones, the coincidence count distributions are in particular affected by this procedure.

This illustrates that the influence of dithering cannot be predicted by the C_V of the underlying spike trains alone. Changes of the coincidence count distribution due to dithering depend on the detailed structure of the interspike interval distribution. For testing if coincidences are occurring by chance, dithering was introduced to eventually destroy existing excess coincidences between neurons to derive the distribution of coincident events occurring by chance. However, since dithering destroys not only coincident events of coupled neurons but also the shape of the coincidence distribution due to changes on the autostructure, it is not possible to tell the one effect from the other. Therefore, significant deviations of the number of coincidences could be due to either changes on the autostructure or the coupling of neurons. This illustrates that dithering, even if very small compared to the expected interspike interval or other methods that manipulate the autostructure of the original spike trains, may lead to false conclusions whether or not excess synchronous activity occurs.

Figure 8: Probability of false positives (test level, 1%) for coincidences shared by a pair of mutually independent gamma processes (A1–A4) or log-normal processes. The statistical significance of a coincidence count of the original pair of processes was evaluated based on dithered versions of the original spike trains. The dithering for each individual spike of the spike trains was randomly distributed following a normal distribution with standard deviation σ_d in milliseconds. The amount of dithering σ_d was varied ($\sigma_d = 5$ ms, $\sigma_d = 10$ ms, $\sigma_d = 20$ ms, $\sigma_d = 40$ ms). In addition the bin width was varied (different rows: A1, B1 $\Delta t = 1$ ms; A1, B1 $\Delta t = 2$ ms; A1, B1 $\Delta t = 3$ ms; A1, B1 $\Delta t = 4$ ms). The firing rate of the processes was 50 Hz in all cases.

The procedure we have taken here provides an average estimate of the effect of manipulation by dithering. However, when estimating the significance of a number of coincidences in a data set, dithering is applied many times to the original data set. Based on the coincidences counted in each dithered version of the original data, the coincidence distribution generated then serves for significance estimation of the number of coincidences found in the original data set (for details see Louis et al., 2010; Louis, Borgelt, & Grün, 2010).

5 Discussion

Coordinated neuronal activity across many neurons is a major component of neuronal activity and involved in neuronal coding. However, the discussion whether coordinated activity really exists and if it is used for coding (Hebb, 1949; Barlow, 1972; Rieke, Warland, de Ruyter van Steveninck, & Bialek, 1997; Shadlen & Movshon, 1999; Singer, 1999; Eggermont, 1990; deCharms & Zador, 2000) remains heated and controversial. While a large and still growing number of studies have confirmed that coordinated neuronal activity like coincidences, spatiotemporal patterns, and avalanches occur more often than expected by chance, other studies have reported the opposite (Baker & Lemon, 2000). A major uncertainty is that it is unknown to what degree statistical features of the individual processes are involuntarily neglected and thus change the likelihood that experimentally observed instances of coordinated neuronal activity can be explained by chance (for a review on these issues, see Grün, 2009).

The existence of an autostructure within spike trains is clear, since neurons have a refractory period after they fire a spike, and they fire often with a temporal structure that is bursty, regular, or periodic. In addition, neuronal firing might not be described by renewal processes but exhibit higher-order dependencies of spike times further in the past (Nawrot et al., 2007). In this letter, we studied the influence of the autostructure of renewal processes on the shape of the coincidence count distribution of pairs of mutually independent point processes. To this end, we derived an analytical expression for the expected mean coincidence count value and the Fano factor of the coincidence counts by the autocorrelation of the coincidences, in particular, for gamma renewal processes with integer shape parameters. We supplemented these results with Monte Carlo estimations of the full shape of the coincidence count distributions for gamma renewal processes with noninteger and integer shape parameters, as well as for renewal processes with log-normal distributed interspike intervals.

Our first major finding is that the width of the coincidence count distribution depends critically and in a nontrivial way on detailed properties of the interspike interval distribution. This is best illustrated by the complex and nonmonotonic dependence of the Fano factor FF_c on the C_V of the interspike intervals for both the gamma and log-normal process (see Figures 4

and 5). The complexity of the FF_c becomes even more apparent when differences in the individual spike rates ΔR, changes in the bin length Δt, or changes in the shape parameter γ are considered. All of these affect the FF_c nonlinearly and nonmonotonically for shape parameters larger than 1.

The second major finding is that the width of the coincidence count distribution characterized by FF_c depends on the detailed properties of the individual point processes. This is demonstrated by differences in the Fano factor for gamma and log-normal processes with identical C_V of the interspike interval distributions (see Figure 5). Still, for both types of processes, we found that C_V values indicative of strong regularity or burstiness lead to a larger Fano factor than for intermediate C_Vs when the firing rates of the processes are identical. Note that the complex and mostly nonmonotonic behavior of the Fano factor for gamma processes as a function of the rate difference ΔR and the order parameter γ requires a precise knowledge of these parameters to allow a prediction of FF_c. This suggests that predictions of the FF_c based on estimated model parameters without knowing the underlying distributions are not trustworthy.

5.1 Interaction of Spike Count Variability and Spike Train Regularity. The Fano factor of the coincidences is mainly determined by two factors: variability in the number of spikes for each of the spike trains and the sharpness of the ISI distribution. If the ISI distribution for both spike trains is very narrow and both processes have the same rate, the following is true: if there is a coincidence at a time $t = t_0$, the probability that there is a second coincidence at a time $t \approx t_0 + \langle t \rangle$ is high, while this probability is low if there is no coincidence at time $t = t_0$. This leads to an increase in the variability of the number of coincidences. A higher variability in the number of spikes of the individual neurons also leads to a larger Fano factor of the coincidences. These effects can be separated by dithering the spike trains by an amount that is large compared to the average ISI. This dithering destroys the fine temporal structure in the spike times but maintains the number of spikes and thus their count variability. Indeed we observed in this case that the FF_c depends on only the Fano factor of the spikes counts FF_s of the two neurons (see equation 4.12).

Since the Fano factor of the spike count is equal to C_V^2 for renewal processes, this allows a qualitative understanding of the width of the distribution of coincident events as a function of the coefficient of variation. As the C_V is decreased from a high value, the effect of lowering the Fano factor of the spike counts FF_s dominates, and the Fano factor of the coincidences FF_c decreases. For small C_V, the effect of the fine temporal structure becomes increasingly important. In the latter case, FF_c increases as C_V is lowered even more. The point where this transition occurs, however, depends strongly on the details of the renewal processes. Note also that the higher likelihood of having a coincidence at time $t \approx t_0 + \langle t \rangle$ given a coincidence at time $t = t_0$ applies only when the two spike trains have almost the same rate. This is

true to a lesser extent when the ratio of the rates is around 1:2 or, in general, $n : m$ (with $n, m \in \mathbb{N}$).

5.1.1 Interaction of Higher Complexity of More Than Two Neurons. So far we have discussed the impact of the interspike interval distribution on the distribution of coincidence counts across pairs of neurons. We extended the analytical calculation for integer gamma processes to higher complexities: triplet, quadruplet, quintuplet, or in general ξ-tuplet coincidences. For triplets, the expected number of coincidences $\langle N_C \rangle$ is given by

$$\langle N_c \rangle = K R_1 R_2 R_3 (\Delta t)^3, \tag{5.1}$$

while their Fano factor, FF_c, satisfies

$$FF_c = \frac{1}{R_1 R_2 R_3 (\Delta t)^3} \sum_k \left[A_k^1 A_k^2 A_k^3 - (R_1 R_2 R_3)^2 (\Delta t)^6 \right]. \tag{5.2}$$

Analogous expressions apply for ξ-tuplets of higher complexities, where the change of the Fano factor is becoming even stronger. Moreover, the direction of the change, whether FF_c increases or decreases, does not stay the same with increasing complexities (data not shown).

5.2 Statistical Inference from Dithering. In order to statistically evaluate the existence of coordinated firing, one needs to define a model that predicts the number of coincidences occurring by chance for mutually independent processes. Different approaches have been taken to derive an approximate model for independent processes from recorded biological spike trains. The approaches can be divided into two classes: approaches that consider the full autostructure of the spiking activity of each individual neuron (Pipa et al., 2007, 2008; Harrison & Geman, 2009) and approaches that ignore, at least partly, the autostructure. Here we explored the approach of dithering (Date et al., 1998; Abeles & Gat, 2001; Hatsopoulos et al., 2003; Shmiel et al., 2006) that belongs in the latter class.

5.2.1 Dithering as Implementation of the Null Hypothesis for Coincidences. Dithering of individual spikes was proposed to test whether coincidences occur by chance. The basic idea is that dithering destroys existing coincident events caused by neuronal coupling. In order to test if in the original data set coincidences occur more often than expected by chance, their number is compared with the distribution of coincidences derived by dithering. Since small amounts of dithering do not alter the rate profile significantly, it was proposed for the detection of synchronized neuronal activity during the presence of rate variation. However, as shown here, dithering not only destroys coincident events induced by coupling, but also changes the

shape of the coincidence distribution due to changes of the autostructure. Therefore, significant deviations from the number of coincidences expected by chance can be due to either changes of autostructure or the coupling of neurons. To judge whether changes of the autostructure are of practical relevance for significance estimation based on dithering, we investigated to what degree FF_c and the shape of the coincidence count distribution change as a function of the amount of dither and the nature of the autostructure of the spike trains.

The amount of dither is constrained by two timescales. The lower bound is given by the bin length Δt. Any change smaller or of the order of Δt has little chance of destroying potentially existing coordinated events (Pazienti et al., 2008). The upper bound is given by the fastest timescale of rate changes present in the data. Therefore, dithering should be chosen of a particular width, for example, from a gaussian distribution with zero mean and variance σ_d^2.

We analytically derived the effect of dithering on the Fano factor of the coincident count distribution FF_c. The main result is that changes of FF_c for changes of σ_d are nonmonotonic and can either decrease or increase the variance of the coincidence count distribution for gamma processes with a shape factor larger than or equal to two. The strongest changes of FF_c occur exactly for the domain $(0.1\langle t \rangle < \sigma_d < \langle t \rangle)$, which is often used to manipulate recorded biological spike trains to get a model for independent firing. To understand the impact of this procedure on the estimation of the statistical significance of coordinated firing, we estimated the probability of false positives. To this end, we estimated the probability of significant coincidence counts of simulated mutually independent gamma or log-normal processes given the coincidence count distributions derived from dithered versions of the spike trains.

We found that false positives were considerably increased for small values of the C_V for both gamma and log-normal processes. For larger values of the $C_V > 1$, only the gamma process expressed an increased level of false positives. Thus, even very small numbers of dithers of less than the expected ISI interval can influence the occurrence of false positives quite strongly. Hence, even alternative dither approaches (Davies et al., 2006) that aim to minimize the number of changes on the spiking data by adapting the amount of jitter by preceding and subsequent ISIs may lead to false conclusions whether synchronous activity occurs by chance or not.

5.2.2 Dithering as Implementation of the Null Hypothesis for Complex Patterns. So far we have discussed the impact of dithering on distributions of coincidences between two neurons. Since dithering has also been applied to derive the statistical significance of higher complexity ξ-tuplets as well as for spatiotemporal patterns (Abeles & Gat, 2001) that can involve many neurons and more than one spike from the same neuron, we also studied the impact of dithering on changes of FF_c for higher complexities of ξ. We

found (data not shown here) for the case of synchronous firing of ξ spikes within n neurons for integer gamma processes that the effect of dithering on the width of the coincidence distribution becomes more pronounced with increasing complexity. However, the direction of the change of FF_c (i.e., whether dithering broadens or narrows the distribution) can be different for different complexities even for the same σ_d and cannot be predicted from the effect of dithering on doublets. However, for most values of C_V, dithering decreases the Fano factor of the coincidence count distribution FF_c for complexities $\xi > 2$. This means that for most values of C_V, dithering leads to an increased level of false positives.

In case of coincident firing that involves maximally one spike per neuron, the expected value of coincident events stays unchanged for different types of autostructures, while the variability of the coincident count distribution changes. In the case of spatiotemporal patterns, which can include more than a single spike from each neuron, the situation is different. Here, the autocorrelation influences the probability of occurrences of a certain spike sequence of the same neuron directly. Hence, any autostructure that deviates from Poissonian firing leads not only to a change of the variance but also to a change of the expected value of the number of spatiotemporal patterns. Whether the expected number is larger or smaller than in case of Poissonian firing depends on the autocorrelation. If the autocorrelation exhibits a bump that corresponds to the interval between spikes of the same neuron in the spatiotemporal pattern, the expected number will be larger than with Poisson processes.

Hence, for spatiotemporal patterns, dithering can alter not only the variance of the count distribution of spatiotemporal patterns but also the expected number. This makes a prediction of changes on the distribution of spatiotemporal pattern due to dithering difficult. However, our results suggest that spike trains that are very regular or bursty have a higher number of chance patterns as compared to Poisson processes. Thus, dithering may trivially reduce the expected number and may generate false positives. Unfortunately, up to now, this has not been investigated. However, it was shown that assuming an incorrect shape factor for surrogate gamma processes (e.g., too low) would also yield a lower expectation for the correct shape factor (Gerstein, 2004). Assuming a shape factor for surrogate data higher than in real data would lead to the opposite conclusion (Baker & Lemon, 2000).

5.2.3 Relation to Other Spike Correlation Analysis Approaches. This study directly relates to other correlation analysis approaches that base their significance evaluation on certain assumptions. For example, the unitary events (UE) analysis (Grün et al., 2002a, 2002b) in its original form assumes Poisson statistics to analyze the significance of coincident spike events (see Grün, 2009, for surrogate-based UE analysis). This assumption enables calculating the coincidence distribution analytically. Thus, given the results in this

letter, one would expect that assuming Poisson processes in the presence of, say, bursty processes would lead to false-positive outcomes in the UE analysis (see Figure 5). However, this is not the case (Grün, 2009). The reason is twofold. First, the UE analysis operates on binned and clipped spike trains, which considerably reduces the burstiness. Second, it adjusts the mean of the coincidence distribution (Poisson) used for the significance evaluation according to the spike counts in the data under evaluation. The comparison of coincidence counts resulting from Poisson and non-Poisson processes we have shown in this study was based on distributions derived from many realizations parameterized by the firing rate of the processes. As a consequence, spike count variations of the various realizations also contribute to the width of the distributions, which UE avoids (see for details, Pipa, van Vreeswijk, & Grün, 2010). Further, the UE analysis for intermediate C_Vs leads to fewer false positives as the applied test level, which explains the enhanced significance of excess spike synchrony found in a comparative analysis of the same data by NeuroXidence and UE (Pipa et al., 2007).

Louis, Gerstein, Grün, and Diesmann (2010) extensively compared various surrogate approaches for the significance estimation of excess spike synchrony in the framework of UE analysis (Grün et al., 2002b). Pairs of spike trains were modeled as gamma processes in nonstationary settings, and the significance of empirically found coincidences was evaluated using surrogate data. Different kinds of spike dithering (mere dither, square root dither, joint-ISI dither, and dithering in operational time) were studied despite the shift procedures used in Pipa et al. (2007). The false-positive level decreased for the methods that increasingly include more features of the original spike trains but still showed an increased FP level for small C_Vs. Thus, the results agree with our findings in this letter for $C_V < 1$ but differ for $C_V > 1$. In that range, FPs were at the expected level (significance level) due to the reasons discussed above for the UE analysis.

6 Conclusion

These results demonstrate that dithering with a dither width much smaller than the average interspike interval can falsify statistical inference of the existence of coordinated neuronal activity. This holds not only for coincidence patterns of two neurons, but also for patterns composed of more neurons or for spatiotemporal patterns. The amount of over- or underestimation of the statistical significance depends on details of the autostructure of the original spike trains and cannot be predicted on the basis of the C_V alone.

Appendix A: List of Symbols Used

t	Interspike interval (ISI)
$p(t)$	ISI distribution
$\langle t \rangle$	Expected value interspike interval t

σ_t^2 Variance of the ISI distribution
R Spike rate $R = \frac{1}{\langle t \rangle}$ in units of spikes per second
C_V Coefficient of variation of the ISI distribution
FF_c Fano factor of the coincidence count distribution
γ Shape parameter of the gamma distribution
a, k Parameter of the log-normal distribution
T Number of trials (realizations) with $t = 1, \dots, T$
Δt Bin width for binning the spike trains, in seconds
T_w Duration of the spike trains in seconds
n_i Spike count in bin i ($n_i \in \mathbb{N}_0$)
N_c Total number of coincidences in interval of $T_w = \Delta t \times I$, corresponding to I bins
$N_{critical}$ Minimal number of coincidences required for significant excess
σ_d^2 Variance of dither distribution
FF_s Fano factor of the spike count distribution

Appendix B: Autocorrelation of the Gamma Process

B.1 Continuous Time. In a γth order gamma process with rate R, the interspike intervals are drawn from from the distribution

$$p(t) = \gamma R \frac{(\gamma R t)^{\gamma - 1}}{(\gamma - 1)!} e^{-\gamma R t}. \tag{B.1}$$

This means that the probability density $p_k(t)$ for the kth spike to occur at time t, given that the zeroth spike occured at time 0, satisfies

$$p_k(t) = \gamma R \frac{(\gamma R t)^{\gamma k - 1}}{(\gamma k - 1)!} e^{-\gamma R t}. \tag{B.2}$$

This can be shown by induction: $p_1(t) = p(t)$, and if p_k satisfies equation B.2, p_{k+1} is given by

$$
\begin{aligned}
p_{k+1}(t) &= \int_0^t p_k(t - t') p(t') dt' \\
&= \frac{(\gamma R)^{\gamma(k+1)}}{(k\gamma - 1)!(\gamma - 1)!} e^{-\gamma R t} \int_0^t (t - t')^{\gamma k - 1} (t')^{\gamma - 1} dt' \\
&= \frac{(\gamma R)^{\gamma(k+1)}}{(k\gamma - 1)!(\gamma - 1)!} e^{-\gamma R t} t^{\gamma(k+1) - 1} \int_0^1 (1 - x)^{\gamma k - 1} x^{\gamma - 1} dx \\
&= \gamma R \frac{(\gamma R t)^{\gamma(k+1) - 1}}{[\gamma(k+1) - 1]!} e^{-\gamma R t},
\end{aligned}
\tag{B.3}
$$

where we have used $\int_0^1 (1 - x)^m x^n dx = m!n!/(n + m)!$

For $t > 0$, the autocorrelation of a spike train, $A(t)$, is given by

$$A(t) = R \sum_{k=1}^{\infty} p_k(t). \tag{B.4}$$

For a γth order gamma process, this is given by

$$A(t) = \gamma R^2 \sum_{k=1}^{\infty} \frac{(\gamma R t)^{\gamma k-1}}{(\gamma k - 1)!} e^{-\gamma R t}$$

$$= \gamma R^2 \sum_{k=1}^{\infty} a_{\gamma,k} \frac{(\gamma R t)^{k-1}}{(k-1)!} e^{-\gamma R t}, \tag{B.5}$$

where $a_{\gamma,k} = 1$ if k is a multiple of γ and $a_{\gamma,k} = 0$ otherwise.

We can write for $a_{\gamma,k}$, $a_{\gamma,k} = \frac{1}{\gamma} \sum_{l=0}^{\gamma-1} x_{\gamma}^{kl}$, where $x_{\gamma} = \exp(2\pi i/\gamma)$. That this choice has the right properties can be seen as follows. If k is a multiple of γ, $x_{\gamma}^k l = 1$ for all l, so that $a_{\gamma,k} = 1$, while if k is not a multiple of γ, $x_{\gamma}^k \neq 1$, but $\gamma (1 - x_{\gamma}^k) a_{\gamma,k} = \sum_{l=0}^{\gamma-1} x_{\gamma}^{kl} - \sum_{l=1}^{\gamma} x_{\gamma}^{kl} = 1 - x_{\gamma}^{\gamma k} = 0$, so that $a_{\gamma,k} = 0$.

Using this parameterization of $a_{\gamma,k}$ one obtains

$$A(t) = R^2 \sum_{k=1}^{\infty} \sum_{l=0}^{\gamma-1} x_{\gamma}^{kl} \frac{(\gamma R t)^{k-1}}{(k-1)!} e^{-\gamma R t}$$

$$= R^2 \sum_{l=0}^{\gamma-1} x_{\gamma}^{l} \sum_{k=1}^{\infty} \frac{(x_{\gamma}^{l} \gamma R t)^{k-1}}{(k-1)!} e^{-\gamma R t}$$

$$= R^2 \left(1 + \sum_{l=1}^{\gamma-1} x_{\gamma}^{l} e^{-(1-x_{\gamma}^{l}) n R t} \right). \tag{B.6}$$

Using $A(-t) = A(t)$ and the contribution of the correlation of each spike with itself, we obtain for the full autocorrelation

$$A(t) = R\delta(t) + R^2 \left(1 + \sum_{l=1}^{\gamma-1} x_{\gamma}^{l} e^{-(1-x_{\gamma}^{l})\gamma R|t|} \right). \tag{B.7}$$

B.2 Binning. We now bin the spikes in bins of width Δt and denote by A_k the average of the product of the number of spikes in bins l and $l+k$:

$$A_k = \int_0^{\Delta t} \int_0^{\Delta t} A(k\Delta t + t_2 - t_1) \, dt_2 \, dt_1. \tag{B.8}$$

For $k = 0$ we have

$$
A_0 = \int_0^{\Delta t} \int_0^{\Delta t} R\delta(t_2 - t_1) + R^2 \left(1 + \sum_{l=1}^{\gamma-1} x_\gamma^l e^{-(1-x_\gamma^l)\gamma R|t_2-t_1|} \right) dt_2\, dt_1
$$

$$
= R\Delta t + (R\Delta t)^2 + 2R^2 \sum_{l=1}^{\gamma-1} x_\gamma^l \int_0^{\Delta t} \int_{t_1}^{\Delta t} e^{-(1-x_\gamma^l)\gamma R(t_2-t_1)}\, dt_2\, dt_1
$$

$$
= R\Delta t + (R\Delta t)^2 \frac{R}{\gamma} \sum_{l=1}^{\gamma-1} \frac{x_\gamma^l}{1 - x_\gamma^l} \int_0^{\Delta t} 1 - e^{(1-x_\gamma^l)\gamma R(t_1-\Delta t)}\, dt_1
$$

$$
= R\Delta t \left(1 + \frac{2}{\gamma} \sum_{l=1}^{\gamma-1} \frac{x_\gamma^l}{1 - x_\gamma^l} \right) + (R\Delta t)^2 - \frac{2}{\gamma^2} \sum_{l=1}^{\gamma-1} \frac{x_\gamma^l \left[1 - e^{-(1-x_\gamma^l)\gamma R\Delta} \right]}{(1 - x_\gamma^l)^2}.
$$

$$(B.9)$$

Using $\frac{x_\gamma^l}{1-x_\gamma^l} = \frac{1}{x_\gamma^{\gamma-l}-1}$ we can write

$$
\sum_{l=1}^{\gamma-1} \frac{x_\gamma^l}{1 - x_\gamma^l} = \sum_{l=1}^{\gamma-1} \frac{1}{x_\gamma^{\gamma-l} - 1} = - \sum_{l=1}^{\gamma-1} \frac{1}{1 - x_\gamma^l}, \tag{B.10}
$$

which can be used to write

$$
\sum_{l=1}^{\gamma-1} \frac{x_\gamma^l}{1 - x_\gamma^l} = \frac{1}{2} \left[\sum_{l=1}^{\gamma-1} \frac{x_\gamma^l}{1 - x_\gamma^l} - \sum_{l=1}^{\gamma-1} \frac{1}{1 - x_\gamma^l} \right]
$$

$$
= \frac{1}{2} \sum_{l=1}^{\gamma-1} \frac{x_\gamma^l - 1}{1 - x_\gamma^l} = -\frac{\gamma - 1}{2}. \tag{B.11}
$$

Thus, A_0 can be written as

$$
A_0 = \frac{R\Delta t}{\gamma} + (R\Delta t)^2 - 2 \sum_{l=1}^{\gamma-1} B_l, \tag{B.12}
$$

with

$$
B_l = \frac{x_\gamma^l}{\gamma^2 (1 - x_\gamma^l)^2} \left(1 - e^{-(1-x_\gamma^l)\gamma R\Delta t} \right). \tag{B.13}
$$

For $k > 0$, one obtains

$$A_k = \int_0^{\Delta t} \int_0^{\Delta t} R^2 \left(1 + \sum_{l-1}^{\gamma-1} x_\gamma^l e^{-(1-x_\gamma^l)\gamma R(k\Delta t + t_2 - t_1)}\right) dt_2\, dt_1$$

$$= (R\Delta t)^2 + R^2 \sum_{l-1}^{\gamma-1} x_\gamma^l e^{-(1-x_\gamma^l)\gamma Rk\Delta t} \int_0^{\Delta t} e^{(1-x_\gamma^l)\gamma R t_1}\, dt_1 \int_0^{\Delta t} e^{-(1-x_\gamma^l)\gamma R t_2}\, dt_2$$

$$= (R\Delta t)^2 + \sum_{l-1}^{\gamma-1} \frac{x_\gamma^l e^{-(1-x_\gamma^l)\gamma Rk\Delta t}}{\gamma^2 (1 - x_\gamma^l)^2} \left[e^{(1-x_\gamma^l)\gamma R\Delta t} + e^{-(1-x_\gamma^l)\gamma R\Delta t} - 2\right].$$

$$\text{(B.14)}$$

For $k < 0$ we can use $A_k = A_{-k}$ so that for $k \neq 0$, A_k is given by

$$A_k = (R\Delta t)^2 + \sum_{l-1}^{\gamma-1} B_l (1 - Z_l) \left[Z_l\right]^{|k|-1} \tag{B.15}$$

with

$$Z_\gamma^l = e^{-(1-x_\gamma^l)\gamma R\Delta t}. \tag{B.16}$$

Appendix C: Estimation of the Coincidence Count Distribution _____

To estimate the coincidence count distribution we used the following procedure:

1. We generate mutually independent pairs of spike trains of length T_w as stochastic realizations of the same underlying process. To this end, we draw iteratively as many interspike intervals t_i from the same underlying ISI distribution $p(\Delta t)$) as needed to cover a period of $T_w + 2\rho$. Hence, two periods, each of length ρ—one preceding T_w and one afterward—are used to randomize the starting conditions (warm-up). ρ was selected to be 500 s. That gives on average 25,000 spikes in the warm-up period for a spike rate of 50 Hz. In addition the first initial interval was drawn from an exponential distribution with the same expected ISI.
2. Binning of the sequence of interspike intervals. We partitioned T_w into $i = 1, \ldots, I$ exclusive bins each of length Δt and counted the number of spikes n_i falling into each individual bin ($n_i \in N_0$).
3. The number of coincidences was derived. To this end, we derived the coincidence count for each individual bin as the product of the

spike counts of corresponding bins i of the first n_i^1 and the second spike train n_i^2. In a last step, we computed the sum of coincidences $N_c = \sum_{i=1}^{I} n_i^a n_i^b$ across all i bins in the interval of T_w.

4. Steps 1 to 4 were iterated T times ("trials") to estimate the probability distribution of $p(N_c)$ by $\hat{p}(N_c)$.

Acknowledgments

References

Abeles, M. (1991). *Corticonics: Neural circuits of the cerebral cortex*. Cambridge: Cambridge University Press.

Abeles, M., Bergman, H., Margalit, E., & Vaadia, E. (1993). Spatiotemporal firing patterns in the frontal cortex of behaving monkeys. *Journal of Neurophysiolology*, *70*(4), 1629–1638.

Abeles, M., & Gat, I. (2001). Detecting precise firing sequences in experimental data. *Journal of Neuroscience Methods*, *107*(1–2), 141–154.

Aertsen, A. M., Gerstein, G. L., Habib, M. K., & Palm, G. (1989). Dynamics of neuronal firing correlation: Modulation of "effective connectivity." *Journal of Neurophysiolology*, *61*(5), 900–917.

Agmon, A. (2012). A novel, jitter-based method for detecting and measuring spike synchrony and quantifying temporal firing precision. *Neural Systems and Circuits*, *2*(1), 5.

Amari, S.-i., Nakahara, H., Wu, S., & Sakai, Y. (2003). Synchronous firing and higher-order interactions in the neuron pool. *Neural Computation*, *15*, 127–142.

Aoki, T., & Aoyagi, T. (2007). Synchrony-induced switching behavior of spike pattern attractors created by spike-timing-dependent plasticity. *Neural Computation*, *19*(10), 2720–2738.

Baker, S. N., & Lemon, R. (2000). Precise spatiotemporal repeating patterns in monkey primary and supplementary motor areas occur at chance level. *J. Neurophysiolology*, *84*, 1770–1780.

Barlow, H. B. (1972). Single units and sensation: A neuron doctrine for perceptual psychology? *Perception*, *1*, 371–394.

Beggs, J. M., & Plenz, D. (2003). Neuronal avalanches in neocortical circuits. *Journal of Neuroscience*, *23*(35), 11167–11177.

Brody, C. D. (1999). Correlations without synchrony. *Neural Computation*, *11*(7), 1537–1551.

Brown, E. N., Kass, R. E., & Mitra, P. P. (2004). Multiple neural spike train data analysis: State-of-the-art and future challenges. *Nature Neuroscience*, 7(5), 456–461.

Burns, B. D., & Webb, A. C. (1976). The spontaneous activity of neurones in the cat's cerebral cortex. *Proceedings of the Royal Society, London B*, *194*, 211–223.

Cox, R., & Lewis, P. (1966). *The statistical analysis of series of events*. London: Methuen.

Date, A., Bienenstock, E., & Geman, S. (1998). *On the temporal resolution of neural activity* (Tech. Rep.). Providence, RI: Division of Applied Mathematics, Brown University.

Davies, R. M., Gerstein, G. L., & Baker, S. N. (2006). Measurement of time-dependent changes in the irregularity of neuronal spiking. *Journal of Neurophysiolology*, *96*, 906–918.

deCharms, R. C., & Zador, A. (2000). Neural representation and the cortical code. *Annu. Rev. Neurosci.*, *23*, 613–647.

Diesmann, M., Gewaltig, M.-O., & Aertsen, A. (1999). Stable propagation of synchronous spiking in cortical neural networks. *Nature*, *402*(6761), 529–533.

Eggermont, J. J. (1990). *The correlative brain*. Berlin: Springer-Verlag.

Farkhooi, F., Strube-Bloss, M. F., & Nawrot, M. P. (2009). Serial correlation in neural spike trains: Experimental evidence, stochastic modeling, and single neuron variability. *Phys. Rev. E*, *79*, 021905.

Gerhard, F., Haslinger, R., & Pipa, G. (2011a). Applying the multivariate time-rescaling theorem to neural population models. *Neural Computation*, *5*(6), 1452–1483.

Gerhard, F., Haslinger, R., & Pipa, G. (2011b). Extraction of network topology from multi-electrode recordings: Is there a small-world effect? *Frontiers in Computational Neuroscience*, *23*.

Gerstein, G. (2004). Searching for significance in spatio-temporal firing patterns. *Acta Neurobiologiae Experimentalis (Warschau)*, *2*(64), 203–207.

Gerstein, G. L., & Mandelbrot, B. (1964). Random walk models for the spike activity of a single neuron. *Biophysical Journal*, *4*(1, pt. 1), 41–68.

Gerstein, G. L., & Perkel, D. H. (1972). Mutual temporal relationships among neuronal spike trains: Statistical techniques for display and analysis. *Biophysical Journal*, *12*(5), 453–473.

Gray, C. M., König, P., Engel, A. K., & Singer, W. (1989). Oscillatory responses in cat visual cortex exhibit inter-columnar synchronization which reflects global stimulus properties. *Nature*, *338*(6213), 334–337.

Grün, S. (2009). Data-driven significance estimation of precise spike correlation. *Journal of Neurophysiology*, *101*, 1126–1140.

Grün, S., Diesmann, M., & Aertsen, A. (2002a). "Unitary events" in multiple single-neuron spiking activity. I. Detection and significance. *Neural Computation*, *14*(1), 43–80.

Grün, S., Diesmann, M., & Aertsen, A. (2002b). "Unitary events" in multiple single-neuron spiking activity. II. Non-stationary data. *Neural Computation*, *14*(1), 81–119.

Grün, S., Diesmann, M., Grammont, F., Riehle, A., & Aertsen, A. (1999). Detecting unitary events without discretization of time. *Journal of Neuroscience Methods*, *94*(1), 67–79.

Gutkin, B. S., Laing, C. R., Colby, C. L., Chow, C. C., & Ermentrout, G. B. (2001). Turning on and off with excitation: The role of spike-timing asynchrony and synchrony in sustained neural activity. *Journal of Computational Neuroscience*, *11*(2), 121–134.

Harrison, M., & Geman, S. (2009). A rate and history-preserving resampling algorithm for neural spike trains. *Neural Computation*, *21*(5), 1244–1258.

Hatsopoulos, N., Geman, S., Amarasingham, A., & Bienenstock, E. (2003). At what time scale does the nervous system operate? *Neurocomputing*, Vol. 52–54, 25–29.

Hebb, D. O. (1949). *The organization of behavior: A neuropsychological theory*. New York: Wiley.

Ikegaya, Y., Aaron, G., Cossart, R., Aronov, D., Lampl, I., Ferster, D., & Yuste, R. (2004). Synfire chains and cortical songs: Temporal modules of cortical activity. *Science*, *304*(5670), 559–564.

Iyengar, S., & Liao, Q. (1997). Modeling neural activity using the generalized inverse gaussian distribution. *Biological Cybernetics*, *77*, 289–295.

Jones, L. M., Depireux, D. A., Simons, D. J., & Keller, A. (2004). Robust temporal coding in the trigeminal system. *Science*, *304*(5679), 1986–1989.

Kass, R. E., Ventura, V., & Brown, E. N. (2005). Statistical issues in the analysis of neuronal data. *Journal of Neurophysiolology*, *94*(1), 8–25.

Kilavik, B. E., Roux, S., Ponce-Alvarez, A., Confais, J., Grün, S., & Riehle, A. (2009). Long-term modifications in motor cortical dynamics induced by intensive practice. *Journal of Neuroscience*, *29*(40), 12653–12663.

König, P. (1994). A method for the quantification of synchrony and oscillatory properties of neuronal activity. *Journal of Neuroscience Methods*, *54*(1), 31–37.

Krahe, R., & Gabbiani, F. (2004). Burst firing in sensory systems. *Nature Reviews Neuroscience*, *5*(1), 13–23.

Kuhn, A., Aertsen, A., & Rotter, S. (2003). Higher-order statistics of input ensembles and the response of simple model neurons. *Neural Computation*, *1*(15), 67–101.

Levine, M. W. (1991). The distribution of the intervals between neural impulses in the maintained discharges of retinal ganglion cells. *Biological Cybernetics*, *65*, 459–467.

Louis, S., Borgelt, C., & Grün, S. (2010). "*Generation and selection of surrogate methods for correlation analysis Connectivity*," in S. Grün & S. Rotter (Eds.), *Analysis of parallel spike trains* Berlin: Springer.

Louis, S., Gerstein, G., Grün, S., & Diesmann, M. (2010). Surrogate spike train generation through dithering in operational time. *Frontiers in Computational Neuroscience*, *4*(127). doi:10.3389/fncom.2010.00127.

Nawrot, M., Boucsein, C., Rodriguez Molina, V., Riehle, A., Aertsen, A., & Rotter, S. (2008). Measurement of variability dynamics in cortical spike trains. *Journal of Neuroscience Methods*, *169*, 374–390.

Nawrot, M. P., Boucsein, C., Rodriguez Molina, V., Aertsen, A., Grün, S., & Rotter, S. (2007). Serial interval statistics of spontaneous activity in cortical neurons *in vivo* and *in vitro*. *Neurocomputing*, *70*, 1717–1722.

Oram, M. W., Wiener, M. C., Lestienne, R., & Richmond, B. J. (1999). Stochastic nature of precisely timed spike patterns in visual system neuronal responses. *J. Neurophysiolology*, *81*(6), 3021–3033.

Pazienti, A., Diesmann, M., & Grün, S. (2007). Bounds of the ability to destroy precise coincidences by spike dithering. *Lecture Notes in Computer Science*, *4729*, 428–437.

Pazienti, A., Maldonado, P., Diesmann, M., & Grün, S. (2008). Effectiveness of systematic spike dithering depends on the precision of cortical synchronization. *Brain Research*, *1225*, 39–46.

Pipa, G., & Grün, S. (2003). Non-parametric significance estimation of joint-spike events by shuffling and resampling. *Neurocomputing*, *52–54*, 31–37.

Pipa, G., & Munk, M. (2011). Higher order spike synchrony in prefrontal cortex during visual memory. *Frontiers in Computational Neuroscience, 5*.

Pipa, G., Riehle, A., & Grün, S. (2007). Validation of task-related excess of spike coincidences based on neuroxidence. *Neurocomputing*, *70*, 2064–2068.

Pipa, G., van Vreeswijk, C., & Grün, S. (2010). *Impact of spike-train auto-structure on unitary events*. Unpublished manuscript.

Pipa, G., Wheeler, D., Singer, W., & Nikolic, D. (2008). Neuroxidence: Reliable and efficient analysis of an excess or deficiency of joint-spike events. *Journal of Computational Neuroscience*, *25*(1), 64–88.

Riehle, A., Grün, S., Diesmann, M., & Aertsen, A. (1997). Spike synchronization and rate modulation differentially involved in motor cortical function. *Science*, *278*(5345), 1950–1953.

Rieke, F., Warland, D., de Ruyter van Steveninck, R., & Bialek, W. (1997). *Spikes: Exploring the neural code*. Cambridge, MA: MIT Press.

Shadlen, M. N., & Movshon, A. J. (1999). Synchrony unbound: A critical evaluation of the temporal binding hypothesis. *Neuron*, *24*, 67–77.

Shmiel, T., Drori, R., Shmiel, O., Ben-Shaul, Y., Nadasdy, Z., Shemesh, M., et al. (2006). Temporally precise cortical firing patterns are associated with distinct action segments. *J. Neurophysiolology*, *96*(5), 2645–2652.

Singer, W. (1999). Neural synchrony: A versatile code for the definition of relations. *Neuron*, *24*, 49–65.

Smith, W. (1954a). Asymptotic renewal theorems. *Proc. Roy. Soc. Edinb. A*, *64*, 9–48.

Smith, W. (1954b). On the cumulants of renewal processes. *Biometrika*, *64*, 1–29.

Sommer, F. T., & Wennekers, T. (2001). Associative memory in networks of spiking neurons. *Neural Netw.*, *14*(6–7), 825–834.

Teich, M. C., Heneghan, C., Lowen, S. B., Ozaki, T., & Kaplan, E. (1997). Fractal character of the neural spike train in the visual system of the cat. *Journal Optical Society America A*, *14*(3), 529–546.

Truccolo, W., Eden, U. T., Fellows, M. R., Donoghue, J. P., & Brown, E. N. (2005). A point process framework for relating neural spiking activity to spiking history, neural ensemble, and extrinsic covariate effects. *Journal of Neurophysiolology*, *93*(2), 1074–1089.

Ventura, V., Cai, C., & Kass, R. E. (2005). Statistical assessment of time-varying dependency between two neurons. *J. Neurophysiolology*, *94*(4), 2940–2947.

Vicente, R., Gollo, L., Mirasso, C. I., Fischer, I., & Pipa, G. (2008). Dynamical relaying can yield zero time lag neuronal synchrony despite long conduction delays. *Proceedings of the National Academy of Science USA*, *105*(44), 17157–17162.

Wu, W., Wheeler, D. W., & Pipa, G. (2011). Bivariate and multivariate neuroxidence: A robust and reliable method to detect modulations of spike-spike synchronization across experimental conditions. *Frontiers in Neuroinformatics*, *5*(August), 1–11.